Article

Current Biology

A distributed auditory network mediated by pontine central gray underlies ultra-fast awakening in response to alerting sounds

Graphical abstract

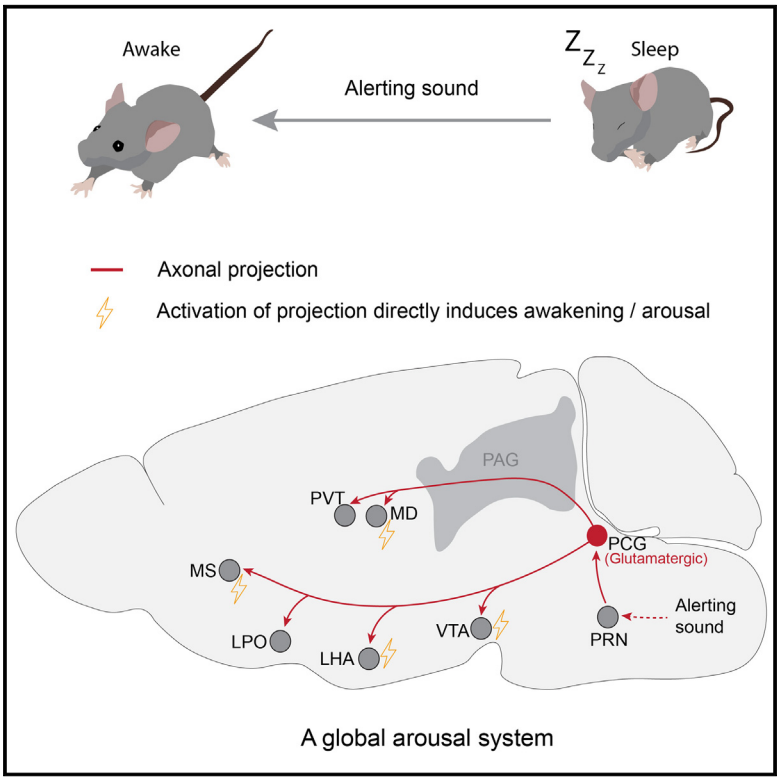

Authors

Jinxing Wei, Cuiyu Xiao, Guang-Wei Zhang, Li Shen, Huizhong W. Tao, Li I. Zhang

Correspondence

htao@usc.edu (H.W.T.), liizhang@usc.edu (L.I.Z.)

In brief

The ability to rapidly wake up from sleep upon threat signals is critical for animal survival. In this study, Wei et al. report that the pontine central gray (PCG) is a critical node of a fast-execution alerting system and globally broadcasts alerting auditory signals to a distributed brain network to promote awakening.

Highlights

- PCG glutamatergic neurons contribute to sound-induced rapid awakening
- They exhibit higher sensitivity in sleep and modulate intrinsic sleep/wake states
- Their activation induces ultra-fast awakening from NREM sleep
- PCG transmits auditory signals to a multitude of arousal-related brain regions

Wei et al., 2024, Current Biology *34*, 4597–4611
October 21, 2024 © 2024 Elsevier Inc. All rights are reserved, including those for text and data mining, AI training, and similar technologies.
https://doi.org/10.1016/j.cub.2024.08.020

CellPress

Current Biology

CellPress

Article

A distributed auditory network mediated by pontine central gray underlies ultra-fast awakening in response to alerting sounds

Jinxing Wei,[1,3] Cuiyu Xiao,[1,3] Guang-Wei Zhang,[1,2] Li Shen,[1] Huizhong W. Tao,[1,2,*] and Li I. Zhang[1,2,4,*]

[1]Zilkha Neurogenetic Institute, Center for Neural Circuits and Sensory Processing Disorders, Keck School of Medicine, University of Southern California, Los Angeles, CA 90033, USA

[2]Department of Physiology and Neuroscience, Keck School of Medicine, University of Southern California, Los Angeles, CA 90033, USA

[3]These authors contributed equally

[4]Lead contact

*Correspondence: htao@usc.edu (H.W.T.), liizhang@usc.edu (L.I.Z.)

https://doi.org/10.1016/j.cub.2024.08.020

SUMMARY

Sleeping animals can be woken up rapidly by external threat signals, which is an essential defense mechanism for survival. However, neuronal circuits underlying the fast transmission of sensory signals for this process remain unclear. Here, we report in mice that alerting sound can induce rapid awakening within hundreds of milliseconds and that glutamatergic neurons in the pontine central gray (PCG) play an important role in this process. These neurons exhibit higher sensitivity to auditory stimuli in sleep than wakefulness. Suppressing these neurons results in reduced sound-induced awakening and increased sleep in intrinsic sleep/wake cycles, whereas their activation induces ultra-fast awakening from sleep and accelerates awakening from anesthesia. Additionally, the sound-induced awakening can be attributed to the propagation of auditory signals from the PCG to multiple arousal-related regions, including the mediodorsal thalamus, lateral hypothalamus, and ventral tegmental area. Thus, the PCG serves as an essential distribution center to orchestrate a global auditory network to promote rapid awakening.

INTRODUCTION

Sleep is characterized by a reduction in behavioral responsiveness to environmental stimuli[1,2] and increased arousal thresholds.[3,4] The ability to rapidly arouse from sleep upon sensory events in a dangerous situation is critical for animal survival.[2,5–11] Although both external stimuli (e.g., tactile, acoustic, and visual)[5,10,12,13] and internal states (e.g., hunger, thirst, and sexual drive)[14] can enhance arousal and affect sleep, relative to internal states, sensory-stimuli-induced awakening from sleep usually exhibits a shorter latency. The properties of sensory stimuli, such as stimulus intensity,[15,16] as well as internal sleep states such as non-rapid eye movement (NREM) and rapid eye movement (REM) sleep, can both have impacts on the probability of awakening.[15] For mammals, the auditory system acts as a crucial, vigilant guardian during sleep, alerting the animal to potential dangers—including approaching predators—and facilitating rapid awakening.[5] However, the neural circuits responsible for sound-induced awakening remain not well understood.

The central auditory system consists of two major ascending pathways. First, the canonical auditory neuroaxis carries auditory information from the cochlear nucleus (CN), to various auditory nuclei in the brainstem, to the medial geniculate nucleus of the thalamus, and finally to the auditory cortex (AC) where auditory perception is generated.[17] Second, the reticular-limbic pathway stems from the CN and navigates through the pontine reticular nucleus (PRN), pontine central gray (PCG), medial septum (MS) before reaching the entorhinal cortex and hippocampus.[18,19] Rather than sound perception, this pathway is thought to be associated with emotion, arousal, attention, and memory[17,18,20] and to play a significant role in the processing of emotionally salient sounds, including those indicative of danger, e.g., loud noise.[18,20] The PCG, a salient structure in the dorsal pons, has been identified as an essential node in this pathway.[17] It is also considered a major component of the ascending reticular activating system (ARAS), which plays a critical role in maintaining arousal and integrating multisensory information.[21–24] Notably, the PCG has been found to respond to multisensory stimuli and provide sensory inputs to the MS in the basal forebrain.[18,25] The latter is involved in modulating cortical electroencephalograms (EEGs) and arousal state.[26–28] These lines of evidence suggest a link between PCG activity and vigilance state, raising a possibility that PCG and its downstream targets may contribute significantly to sound-induced awakening.

By exploring PCG-mediated central auditory pathways, our study reveals that this structure plays an essential role in transmitting auditory signals and facilitating rapid sleep-to-wake transitions upon alerting acoustic events. More specifically, its glutamatergic neurons mediate the sound-induced awakening: optogenetic activation of these neurons induces sleep-to-wake transitions with extremely short latencies, whereas inactivation

All rights are reserved, including those for text and data mining, AI training, and similar technologies.

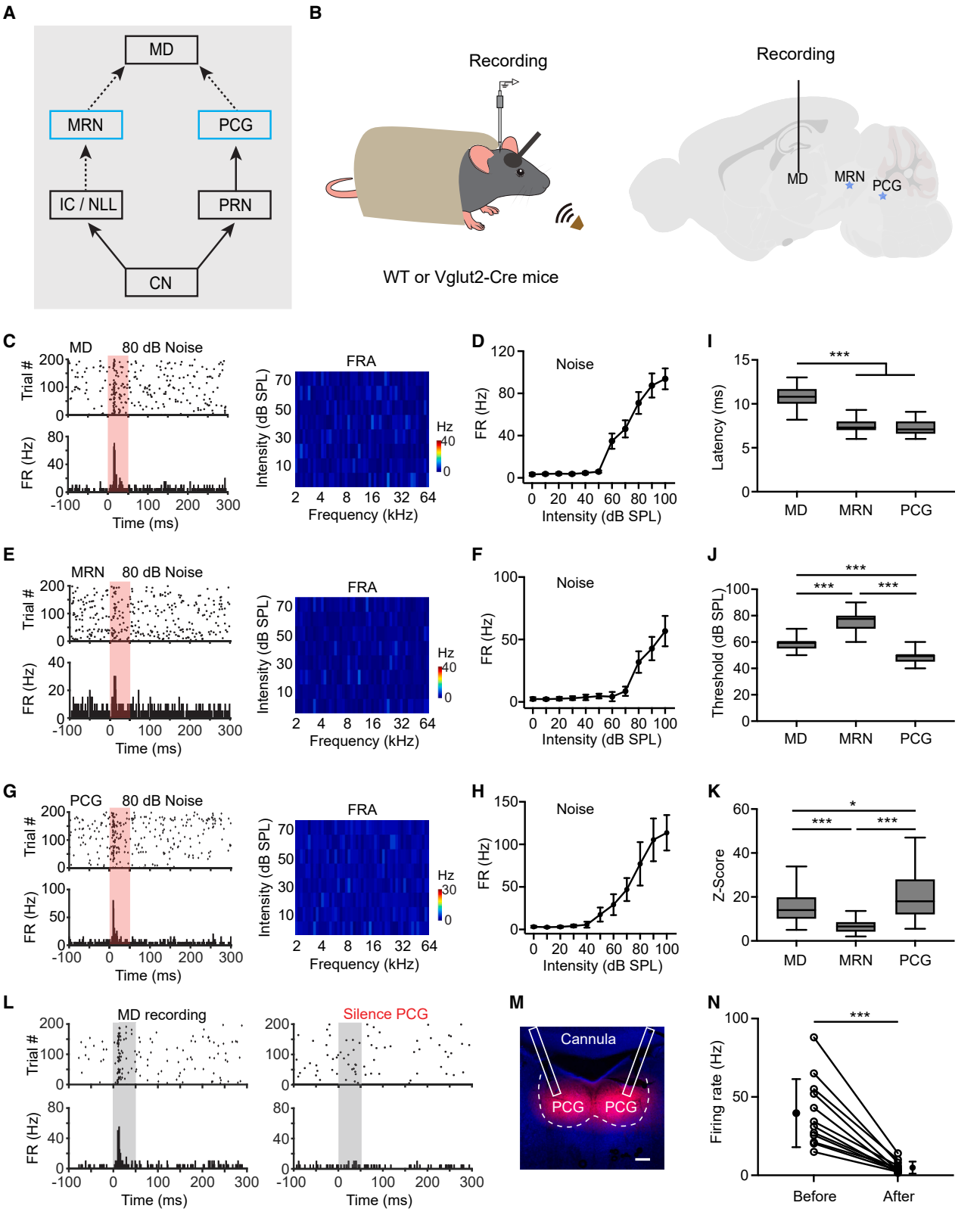

(legend on next page)

CellPress

of them reduces the probability of sensory-induced awakening from sleep. These neurons also contribute to auditory-induced awakening from anesthesia. In addition, we found that the baseline activity of these neurons correlates with intrinsic sleep/wake states: they are more active during wakefulness than during sleep. Silencing of these neurons reduces wakefulness and increases sleep during natural sleep/wake cycles. Furthermore, these PCG glutamatergic neurons elevate their sensitivity to auditory stimuli during NREM sleep relative to wakefulness. Finally, the PCG transmits auditory signals to a multitude of arousal-related brain regions, including the mediodorsal nucleus of the thalamus (MD), lateral hypothalamic area (LHA), and ventral tegmental area (VTA), which contributes to its wake-promoting effect. Together, our results suggest that the PCG serves as an important hub of ascending brainstem circuits to broadcast auditory signals to a large, distributed arousal system and to mediate rapid sound-induced awakening from sleep.

RESULTS

PCG is a primary auditory input source to the MD

As the MD has recently been suggested to be involved in sound-induced arousal from slow-wave sleep,[29] this structure provides an entry point when we explore the neural pathways for auditory-induced awakening. Two routes may potentially convey auditory information to the MD (Figure 1A). First, the MD may receive input from the mesencephalic area (equivalent to the midbrain reticular nucleus, MRN),[29] which is hypothesized to receive input from the inferior colliculus (IC)[29] and/or the nucleus of the lateral lemniscus (NLL)[30] along the canonical auditory neuroaxis. Second, the observation that the MD receives substantial axonal projections from the PCG[20] suggests that the MD may receive auditory signals from the PCG and be part of the reticular-limbic pathway along which the PCG receives input from the PRN and the latter from the CN.[18] To decipher the source of auditory input to the MD, we examined auditory responses in the MD, MRN, and PCG of awake, head-fixed mice with multichannel single-unit recordings (Figure 1B). Auditory stimuli (white noise of varying intensities and pure tones of varying frequencies and intensities) were delivered through a speaker in the contralateral field. Figure 1C shows spike response properties of an example MD neuron. It exhibited a phasic response to noise bursts with an onset latency of 13 ms (Figure 1C, left). By contrast, it did not respond well to pure tones and no clear frequency-responsive area (FRA) was detected (Figure 1C, right). The intensity threshold for the noise response was at around 50–60 dB sound pressure level (SPL) (Figure 1D). Overall, noise-evoked spike responses were observed in about 33.3% (29 out of 87) of recorded MD neurons (Figure S1B). In comparison to MD, MRN neurons appeared to respond less well to noise, without responding to tones (Figure 1E). In the noise-responsive MRN population (34.4%, 42 out of 122 cells) (Figure S1C), the neurons exhibited a much higher intensity threshold than those in the MD, at approximately 70–80 dB SPL (Figure 1F). This suggests that in naive conditions MRN is unlikely a major input source to drive auditory responses of MD neurons.

The PCG consists of two primary neuronal types: glutamatergic (Vglut2+) and GABAergic (Vgat+).[20] In order to be able to identify cell types, we performed optrode recording in Vglut2-Cre animals injected with adeno-associated virus (AAV) encoding Cre-dependent channelrhodopsin 2 (ChR2), following our previous study.[20] Out of 195 units recorded in PCG, 105 neurons were identified as Vglut2+ (i.e., opto-tagged) neurons and 60% of them (63/105) were activated by noise stimuli, with an apparently moderate intensity threshold (Figures 1G and 1H). For the remaining non-tagged cells, only 8.9% (8/90) responded to noise stimuli (Figure S1A), which is consistent with our previous finding that GABAergic PCG neurons essentially do not respond to noise sounds.[20] Thus, the overall fraction of responsive neurons in PCG is 36.4% (71/195) (Figure S1A). For this responsive population, a significantly shorter response latency (Figure 1I), lower intensity threshold (Figure 1J), and higher response level (Figure 1K) was observed compared with MD neurons. By contrast, MRN neurons exhibited a much higher intensity threshold and lower response level than those in the MD (Figures 1J and 1K). Together, these data suggest that, in naive conditions, the PCG is much better positioned than the MRN to deliver auditory information to the MD. To test this possibility, we pharmacologically silenced the PCG by administering muscimol, an agonist of GABA receptors, via implanted cannulas. We found that the

Figure 1. A potential auditory circuit to the MD

(A) Potential auditory circuits to the MD. Solid line indicates confirmed connectivity, while dashed line represents undetermined connectivity.

(B) Left: schematic of recording setup. Right: diagram showing multichannel recording sites in MD and MRN of wild-type animals or optrode recording in PCG of Vglut2-Cre animals.

(C) Left: raster plot (upper) and peri-stimulus spike-time histogram (PSTH) of spike responses to white noise (80 dB SPL, 50 ms) for an example MD neuron. Pink shade marks the duration of sound stimulation. Right: color-coded spike rates in response to tones of different frequencies and intensities (i.e., frequency response area, FRA) for the same cell shown on the left.

(D) Spike rates evoked by noise at different intensity levels (i.e., rate-intensity function) averaged for the responsive neurons in MD (n = 20 cells).

(E) Similar to (C) but for an MRN neuron.

(F) The average rate-intensity function for MRN neurons (n = 24 cells).

(G) Similar to (C) but for a PCG neuron.

(H) The average rate-intensity function for PCG neurons (n = 21 cells).

(I–K) Average onset latency of spike responses to noise (at 80 dB SPL) (I), average intensity threshold (J), and mean response level (at 80 dB SPL) (K) for MD, MRN, and PCG neurons. *p < 0.05, ***p < 0.001, one-way ANOVA and Tukey's post hoc test; n = 29 in MD, 42 in MRN, and 71 in PCG.

(L) Raster plot (upper) and PSTH (lower) of spikes for an example neuron in MD before (left) and after (right) silencing PCG with muscimol. Gray shade marks the duration of noise stimulation.

(M) Representative confocal image of fluorescent muscimol in PCG. Scale bar, 200 μm.

(N) Noise-evoked firing rates of MD neurons before and after silencing PCG with muscimol. ***p < 0.001, paired t test, n = 12 cells.

All error bars represent SD.

See also Figures S1 and S2.

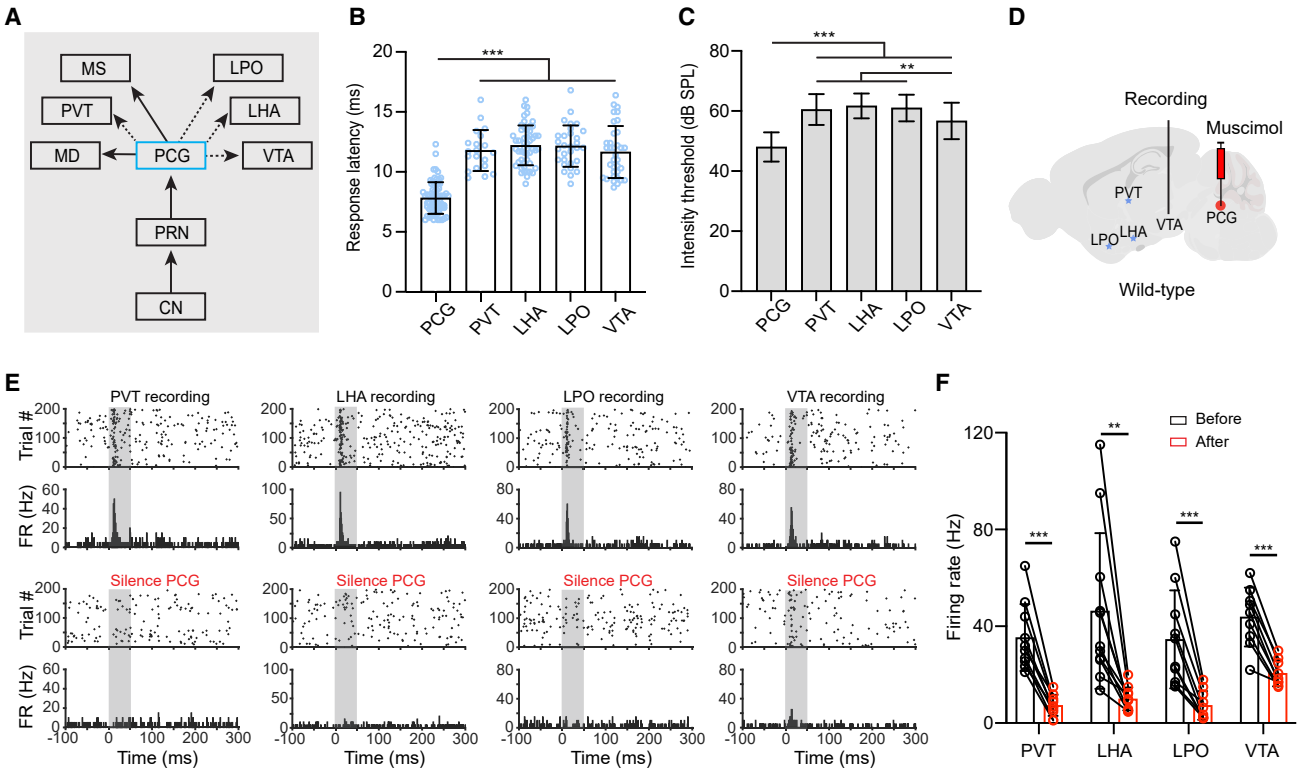

Figure 2. PCG transmits auditory signals to a multitude of brain regions

(A) Potential circuits for the propagation of auditory signals via PCG. Solid line indicates a confirmed pathway, while dashed line represents an unconfirmed pathway.

(B and C) Comparison of onset latency of spike responses to noise (at 70 dB SPL) (B) and intensity threshold (C) for evoking a response among different brain regions. $^{**}p < 0.01$, $^{***}p < 0.001$, one-way ANOVA and Tukey's post hoc test; $n = 71$ cells in PCG, 53 in LHA, 30 in LPO, 20 in PVT, and 35 in VTA.

(D) Schematic of recording in each PCG target region while silencing PCG with muscimol.

(E) Raster plot and PSTH of spikes for an example neuron in PVT, LHA, LPO, and VTA, respectively, before (upper) and after (lower) silencing PCG with muscimol. Gray shade marks the duration of noise stimulation.

(F) Noise-evoked firing rates before and after silencing PCG in different target regions. $^{**}p < 0.01$, $^{***}p < 0.001$, paired t test; $n = 10$ cells in PVT, 11 in LHA, 10 in LPO, and 9 in VTA.

All error bars represent SD.

See also Figure S2.

response to auditory noise in the MD was markedly decreased as compared with the pre-administration condition (Figures 1L–1N). This result confirms that auditory responses in the MD are primarily driven by the input from the PCG.

The PCG broadcasts auditory information to a distributed brain network

Previous anatomical results have indicated that PCG axons project profusely to a multitude of brain regions, encompassing not only the MD but also the MS, paraventricular nucleus of the thalamus (PVT), LHA, lateral preoptic area (LPO), and VTA.[20] We wondered whether, similar to the MD (Figures 1L–1N) and MS,[18] the PCG could also drive auditory responses in these other target regions (Figure 2A). We thus carried out multichannel recordings in the PVT, LHA, LPO, and VTA (Figure S2). Neurons in these regions also exhibited responses to auditory noise. The response latencies and intensity thresholds were comparable among these regions but were all significantly longer and higher than those in the PCG (Figures 2B and 2C). We further silenced the PCG with muscimol (Figure 2D) and found that the auditory responses in the PVT, LHA, LPO, and VTA were all markedly decreased (Figures 2E and 2F). These results thus support the notion that the PCG serves as an important hub in the ascending pontine auditory pathway by broadcasting auditory information to a large, distributed brain network (Figure 2A).

PCG plays a crucial role in sound-induced awakening from sleep

Because the multiple PCG targets, including the VTA, PVT, LHA, LPO, and MD, are related to arousal,[29,31–35] we wondered whether PCG could play a role in sensory-induced awakening, in particular, upon unexpected acoustic events. To test this possibility, we monitored the sleep/wake state in freely moving mice with simultaneous electroencephalogram (EEG) and electromyography (EMG) recordings (Figure 3A). The mice were subjected to intermittent sound stimuli (white noise, 1-s duration at 30–70 dB SPL, with 60–180 s inter-stimulus intervals; STAR Methods). The auditory stimulation could result in rapid

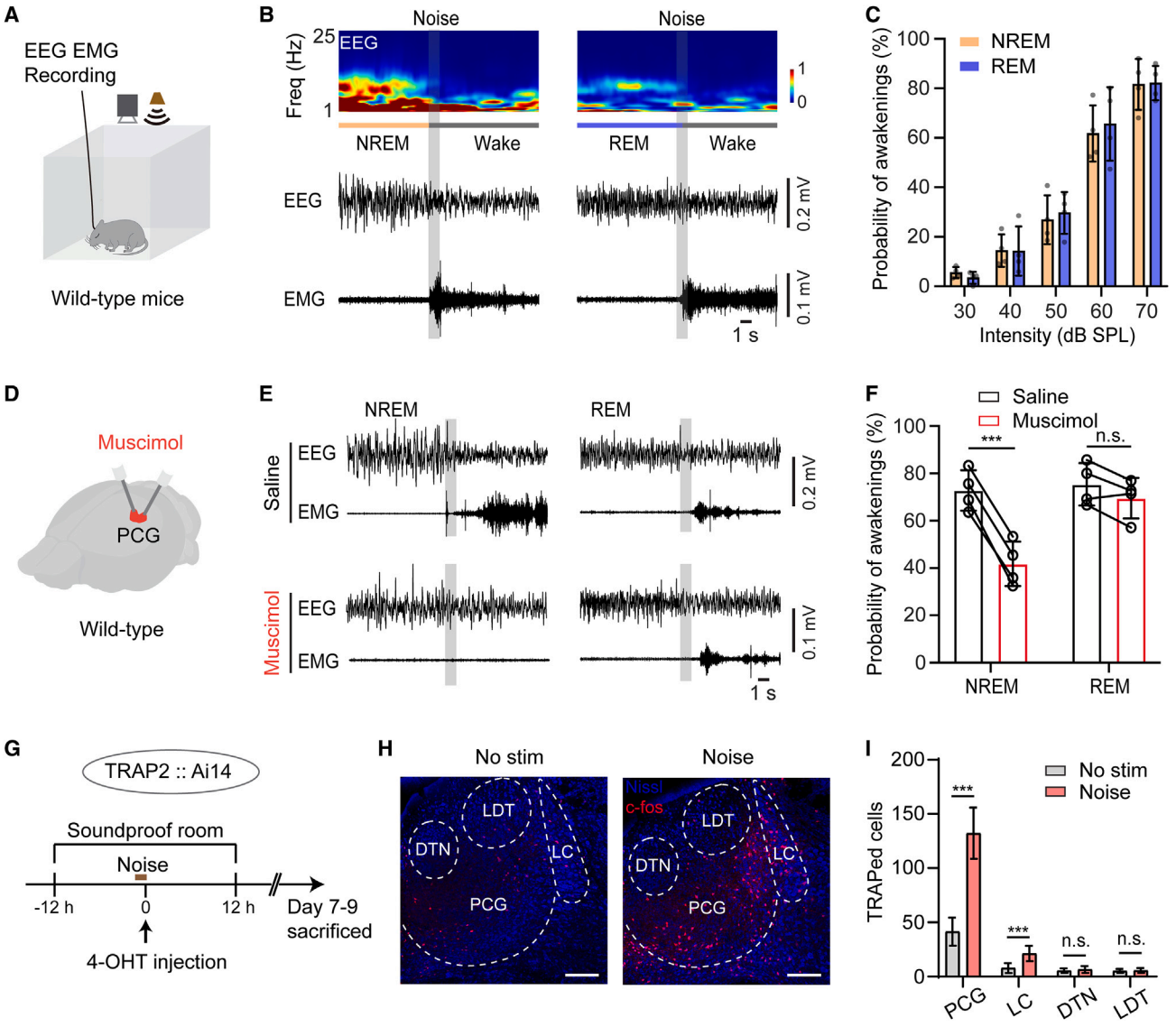

Figure 3. PCG contributes to sound-induced awakening from sleep

(A) Experimental setup. Noise was delivered from the speaker on top of the testing chamber, and the freely moving mouse was continuously monitored with EEG, EMG, and video recording.

(B) Representative EEG power spectrum (top), EEG (middle), and EMG (bottom) traces from a mouse showing a transition to wakefulness from NREM (left) or REM sleep (right). Vertical gray bar marks the duration of noise sound (60 dB SPL). Scale bar, 1 s.

(C) Average probability of awakening (%) from NREM (orange, $n = 4$ mice) or REM sleep (purple, $n = 4$ mice) induced by noise at different intensities. Black circles represent data of individual subjects.

(D) Schematic silencing of PCG with muscimol in wild-type mice.

(E) Representative EEG and EMG traces for an example mouse in the saline control (upper) vs. muscimol (lower) silencing condition. Gray box marks noise (60 dB SPL, 1-s duration) stimulation. Scale bar, 1 s.

(F) Probability of awakening (%) from NREM (left, $n = 4$ mice) or REM sleep (right, $n = 4$ mice) induced by noise in the saline and muscimol condition. ***$p < 0.001$; n.s., not significant, $p > 0.05$, paired t test.

(G) Experimental timeline for TRAPing. A TRAP2::Ai14 mouse was placed in a soundproof room and was given an injection of 4-OHT (50 mg/kg) after 60-min noise stimulation. After 7–9 days, the animal was sacrificed.

(H) Representative confocal images of the PCG and its surrounding structures in mice that received no noise stimulation (left) or received noise stimulation (right). Scale bar, 200 μm. Red, tdTomato-indicative c-*fos* expression.

(I) Quantification of the number of TRAPed cells in different brain regions ($n = 3$ mice for each brain region). ***$p < 0.001$, t test.

All error bars represent SD.

See also Figure S3.

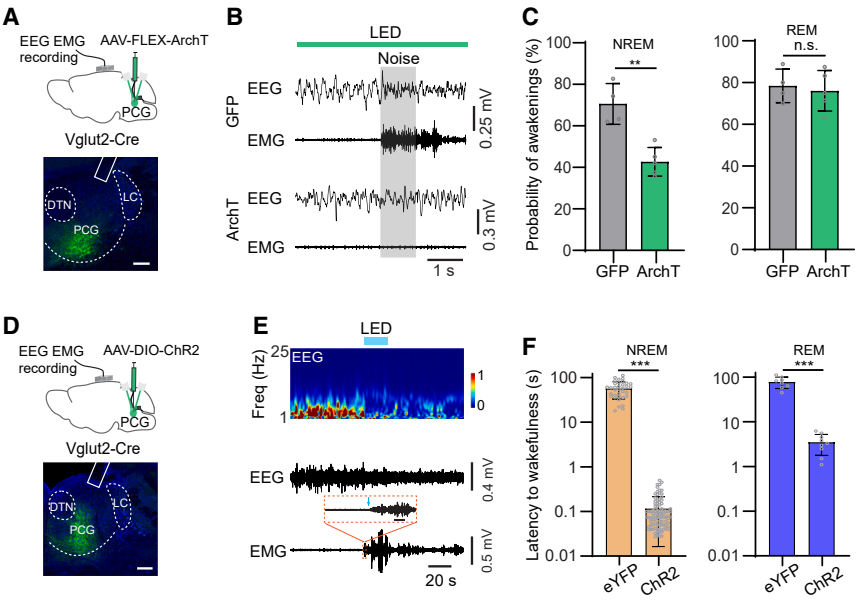

Figure 4. Optogenetic silencing and activation of PCG glutamatergic neurons

(A) Top: schematic viral injection for optogenetic silencing of PCG glutamatergic neurons in Vglut2-Cre mice. Bottom: example image showing ArchT expression and location of the optical fiber in the PCG. Scale bar, 200 μm.

(B) EEG and EMG traces for an example GFP control (upper) and ArchT-expressing (lower) mouse. Gray box marks noise (60 dB SPL, 1-s duration) stimulation. Green line marks green LED light illumination.

(C) Average probability of awakening from NREM (left) or REM sleep (right) induced by noise. NREM, $^{**}p < 0.01$; REM, $p > 0.05$, t test; $n = 4$ and 5 mice for GFP and ArchT group, respectively.

(D) Top: schematic viral injection for optogenetic activation of PCG glutamatergic neurons. Bottom: example image for ChR2 expression. Scale bar, 200 μm.

(E) Representative EEG power spectrum, EEG and EMG traces for a ChR2-expressing animal. Blue line marks LED stimulation (at 20 Hz, for 20 s). Insert: zoomed-in EMG signals (scale bar, 200 ms), with blue arrow depicting the onset of LED stimulation.

(F) Latency to wakefulness from NREM sleep (left) or REM sleep (right) after the onset of LED stimulation. $^{***}p < 0.001$, t test; NREM, $n = 4$ and 6 mice for eYFP and ChR2 group, respectively; REM, $n = 3$ and 4 mice for eYFP and ChR2 group, respectively; each dot indicates one single trial.

All error bars represent SD.

See also Figures S2 and S3.

awakening from both NREM (Figure 3B, left) and REM (Figure 3B, right) sleep, with the probability of induced awakening monotonically increased with increasing sound intensities (Figure 3C). The probability did not differ between the first and second half of the test session (Figure S3A), suggesting a lack of adaptation. The latency to wakefulness was 52 ± 29 ms for NREM sleep and 802 ± 400 ms for REM sleep at the noise intensity of 70 dB SPL. To examine the involvement of the PCG in this sensory-evoked awakening, we locally administered muscimol to PCG (Figure 3D) and found that the probability of the induced awakening from NREM sleep, but not REM sleep, was significantly decreased compared with saline control (Figures 3E and 3F). For successful awakening trials, the latency to wakefulness from NREM sleep was prolonged, whereas that from REM sleep was not changed significantly (saline, 1.38 ± 0.36 s; muscimol, 1.43 ± 0.52 s, at noise intensity of 60 dB SPL; t test, $p = 0.69$, $n = 4$ mice). These results suggest that the PCG may contribute critically to auditory-induced awakening from NREM sleep.

Using the targeted recombination in active populations (TRAPs) strategy,[36–38] we examined neuronal activation patterns in TRAP2 crossed with Ai14 (Cre-dependent tdTomato) mice following 60-min noise stimulation during the light cycle (Figure 3G). After days of expression, we found a marked increase in the number of tdTomato+ (i.e., TRAPed) cells in PCG compared with control mice that had not experienced the noise stimulation (Figures 3H and 3I). This increased neuronal activation is consistent with the PCG's responsiveness to the sound stimuli and may also reflect heightened arousal due to the noise exposure. Increased neuronal activation was also observed in the locus coeruleus (LC), which nevertheless had a much smaller number of TRAPed cells compared with the PCG (Figure 3I). Notably, some other salient nuclei in the dorsal pons, such as the dorsal tegmental nucleus (DTN) and laterodorsal tegmental (LDT), which have been reported to be involved in sleep-wake regulation,[39,40] did not show significant neuronal activation by the noise stimulation (Figure 3I). These results highlight the PCG as a distinct dorsal pontine nucleus crucially involved in auditory-driven awakening.

PCG glutamatergic neurons contribute to auditory-induced awakening

Because PCG's GABAergic neurons essentially do not respond to noise sounds,[20] we examined whether its glutamatergic neurons might play a role in the induction of wakefulness by the noise stimulation. To this end, we optogenetically suppressed these neurons by bilaterally injecting AAV encoding Cre-dependent archaerhodopsin (ArchT) (or GFP as control) into the PCG of Vglut2-Cre mice (Figure 4A). Green light-emitting diode (LED) light was delivered through implanted optic fibers for a continuous 5-s duration that covered the noise stimulation (Figure 4B). Compared with GFP control, the optical inhibition of PCG glutamatergic neurons significantly decreased the probability of auditory-induced awakening (Figure 4C) and increased the latency to wakefulness (Figure S3B) from NREM sleep, which is consistent with the muscimol silencing result. The induced awakening from REM sleep was not affected (Figures 4C and S3C). These results indicate that PCG glutamatergic neurons make an essential contribution to auditory-induced awakening from NREM sleep.

Activation of PCG glutamatergic neurons induces a rapid transition from sleep to wakefulness

We next tested the effect of directly activating PCG glutamatergic neurons on sleep by injecting AAV encoding Cre-dependent ChR2 (or eYFP as control) into the PCG of Vglut2-Cre mice (Figure 4D). Testing was performed during the light cycle of the animals in which blue LED stimulation (5-ms duration at 20 Hz) was

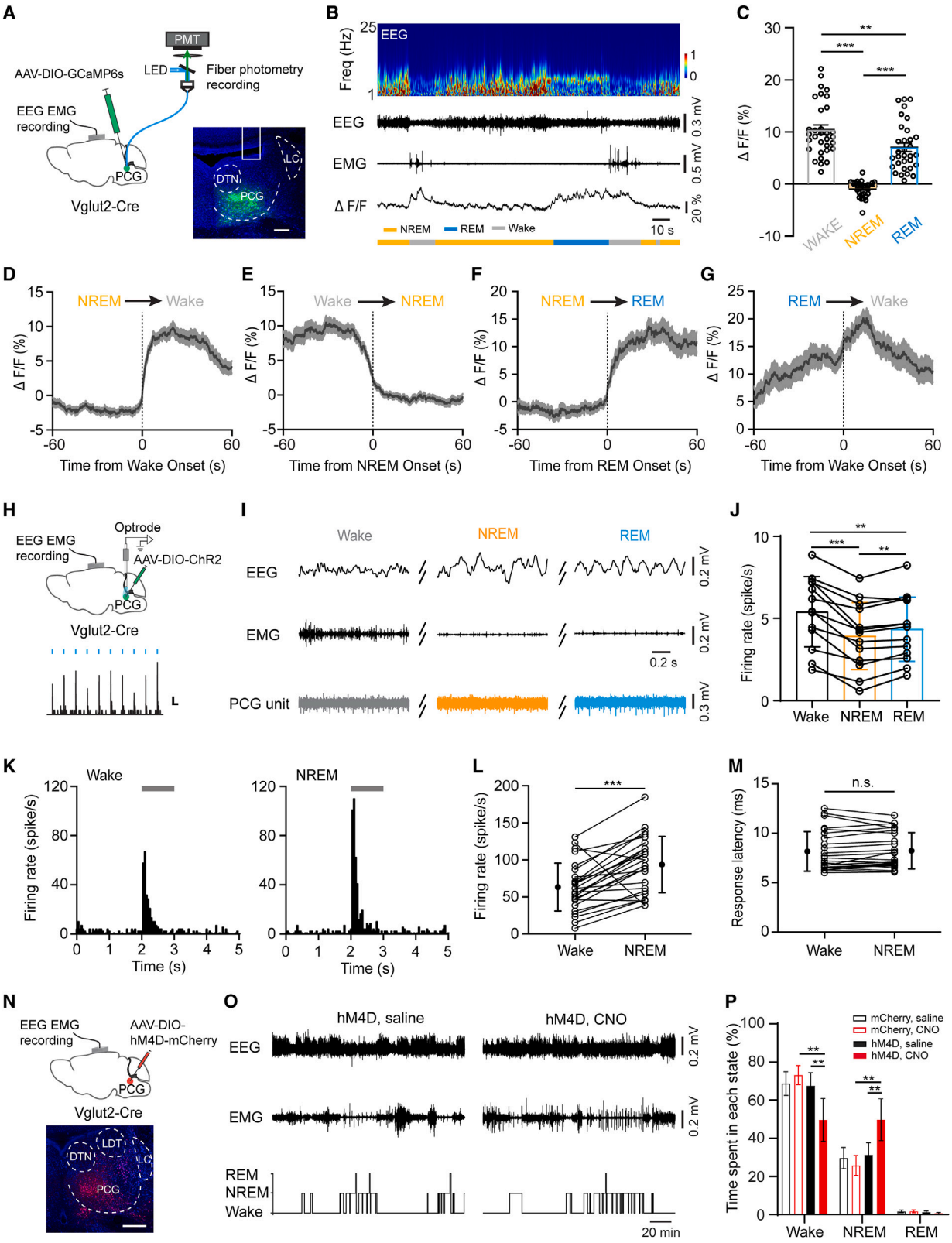

Figure 5. Activity of PCG glutamatergic neurons modulates intrinsic sleep-wake cycles

(A) Experimental condition: AAV1-Syn-FLEX-GCaMP6s was injected into PCG, and fiber photometry and EEG/EMG recordings were performed in Vglut2-Cre mice. The right image shows GCaMP expression and placement of the optic fiber in an example mouse. Scale bar, 200 μm.

(legend continued on next page)

applied for 20 s (Figure 4E). Optical stimulation in both NREM and REM sleep states induced rapid transitions to wakefulness in ChR2-expressing, but not eYFP control, mice (Figure 4F). Nevertheless, the latency to wakefulness was noticeably longer for REM than NREM sleep, differing by one order of magnitude (Figure 4F).

Activity of PCG glutamatergic neurons is modulated by the sleep/wake state

We further examined whether the activity of PCG glutamatergic neurons might be correlated with the natural sleep/wake state by performing fiber photometry recording in freely moving mice (STAR Methods). AAV encoding a Cre-dependent fluorescence Ca^{2+} indicator, GCaMP6s, was injected into PCG of Vglut2-Cre mice and an optic fiber was implanted above the PCG to record ensemble Ca^{2+} signals (Figure 5A). The sleep/wake state was monitored by simultaneous EEG and EMG recordings (Figure 5B). We found that the population Ca^{2+} activity of the glutamatergic neurons was overall higher during wakefulness than sleep and was higher during REM than NREM sleep (Figure 5C). In addition, these neurons began to increase their activity at sleep-to-wake transitions (Figures 5D and 5G) but decreased their activity at wake-to-sleep transitions (Figure 5E). Their activity was also increased at NREM sleep-to-REM sleep transitions (Figure 5F).

We next performed optrode recordings from ChR2-tagged PCG glutamatergic neurons in head-fixed mice across natural sleep-wake cycles. Vglut2+ neurons were identified by their time-locked spike responses to LED light pulses (Figure 5H), following our previous studies.[20,25,41,42] Consistent with the Ca^{2+} imaging data, these neurons exhibited a higher baseline firing rate during wakefulness than during sleep and a higher rate during REM than NREM sleep (Figures 5I and 5J). These data demonstrate that the activity of PCG glutamatergic neurons is dynamically modulated by the sleep/wake state and is highest during wakefulness.

We also examined auditory responses of PCG glutamatergic neurons in different sleep/wake states. In our recording, the majority (65%, 26/40) of PCG glutamatergic neurons reliably responded to noise stimulation with transient spiking in both wakefulness and sleep (Figure 5K). The evoked firing rate displayed an opposite trend to the spontaneous firing rate, that is, it was lower during wakefulness than during NREM sleep (Figure 5L). The onset latency of the auditory responses, however, did not differ between wakefulness and NREM sleep (Figure 5M). For the remaining (35%, 14/40) neurons that were unresponsive to noise during wakefulness, 93% (13/14) of them remained unresponsive during sleep, whereas one neuron became responsive. Thus, the number of responsive neurons slightly increased from wakefulness to NREM sleep. The overall enhanced auditory responsiveness of PCG glutamatergic neurons during sleep may facilitate their functional role in promoting sound-induced awakening.

PCG glutamatergic neurons modulate intrinsic sleep-wake cycles

To investigate the involvement of PCG glutamatergic neuron activity in regulating intrinsic sleep/wake cycles, we used a chemogenetic approach to inhibit these neurons during polysomnographic recordings. AAV encoding an inhibitory DREADD receptor (hM4Di, or mCherry as control) was injected into the PCG of Vglut2-Cre mice (Figure 5N). The DREADD agonist, clozapine-N-oxide (CNO, or saline as control), was administered 30 min before the test in the dark cycle of the animals. During a 3-h test session, the chemogenetic inhibition of PCG glutamatergic neurons led to significantly reduced total time in wakefulness and increased total time in NREM sleep as compared with mCherry control animals or hM4Di-expressing animals injected with saline (Figures 5O and 5P). This was accompanied by a prolonged duration of NREM sleep episodes, a shortened duration of wake episodes, and a slightly increased number of wake episodes (Figure S4). As REM sleep accounted for only a very small fraction of sleep time (Figure 5P), the overall sleep time was increased by the inhibition of PCG glutamatergic neurons. Therefore, the activity of PCG glutamatergic neurons contributes to maintaining wakefulness in normal physiological conditions.

PCG glutamatergic neurons contribute to sound-induced awakening from anesthesia

We wondered whether PCG glutamatergic neurons could also play a role in awakening from anesthesia. To test this possibility, mice were exposed to isoflurane in a closed chamber (Figure 6A).

(B) EEG power, EEG/EMG recording, and photometry recording (ΔF/F) for an example animal during spontaneous sleep/wake transitions. Freq, frequency. Color bars at the bottom label different states (gray, wakefulness; orange, NREM sleep; blue, REM sleep).
(C) Quantification of average ΔF/F during different sleep/wake states (n = 4 mice, 8 sessions per mouse). Each animal was tested for 2–3 sessions per day and each session lasted for 1 h. $^{**}p < 0.01$, $^{***}p < 0.001$, one-way ANOVA and Tukey's post hoc test.
(D–G) Changes in fluorescence signals aligned to the transition between different states. Data represent mean (solid black) ± SEM (shade). n = 4 mice.
(H) Top: schematic viral injection and optrode recording in PCG. Bottom: PSTH for spikes of an example ChR2-tagged PCG glutamatergic neuron in response to LED light pulses (5-ms duration at 10 Hz, marked by blue dots). Scale bars, 10 Hz and 50 ms.
(I) Example EEG, EMG, and PCG unit recording traces during wakefulness, NREM sleep, and REM sleep.
(J) Average firing rates of PCG glutamatergic neurons in different sleep/wake states. Data points for the same neuron are connected with lines. $^{**}p < 0.01$, $^{***}p < 0.001$, one-way ANOVA and Tukey's post hoc test, n = 13 neurons.
(K) PSTH for auditory-evoked spikes of an example PCG glutamatergic neuron during wakefulness (left) and NREM sleep (right). Gray bar marks 1-s noise stimulation (at 60 dB SPL).
(L) Mean auditory-evoked firing rates of PCG glutamatergic neurons in different states. $^{***}p < 0.001$, paired t test, n = 26 cells.
(M) Onset latencies of auditory-evoked responses of PCG glutamatergic neurons in different states. $p > 0.05$, paired t test, n = 26 cells.
(N) Top: schematic viral injection. Bottom: example image showing hM4D expression in PCG. Scale bar, 200 μm.
(O) EEG/EMG traces and hypnogram (bottom) during a 3-h test window after saline (left) or CNO (right, 1 mg/kg) injection for a hM4D-expressing mouse.
(P) Percentage time spent in each state. $^{**}p < 0.01$, two-way ANOVA and least significant difference (LSD) post hoc test, n = 3 and 5 mice for mCherry and hM4D group, respectively.
Error bars represent SEM in (D)–(G) and SD in (C), (J), (L), (M), and (P).
See also Figures S2 and S4.

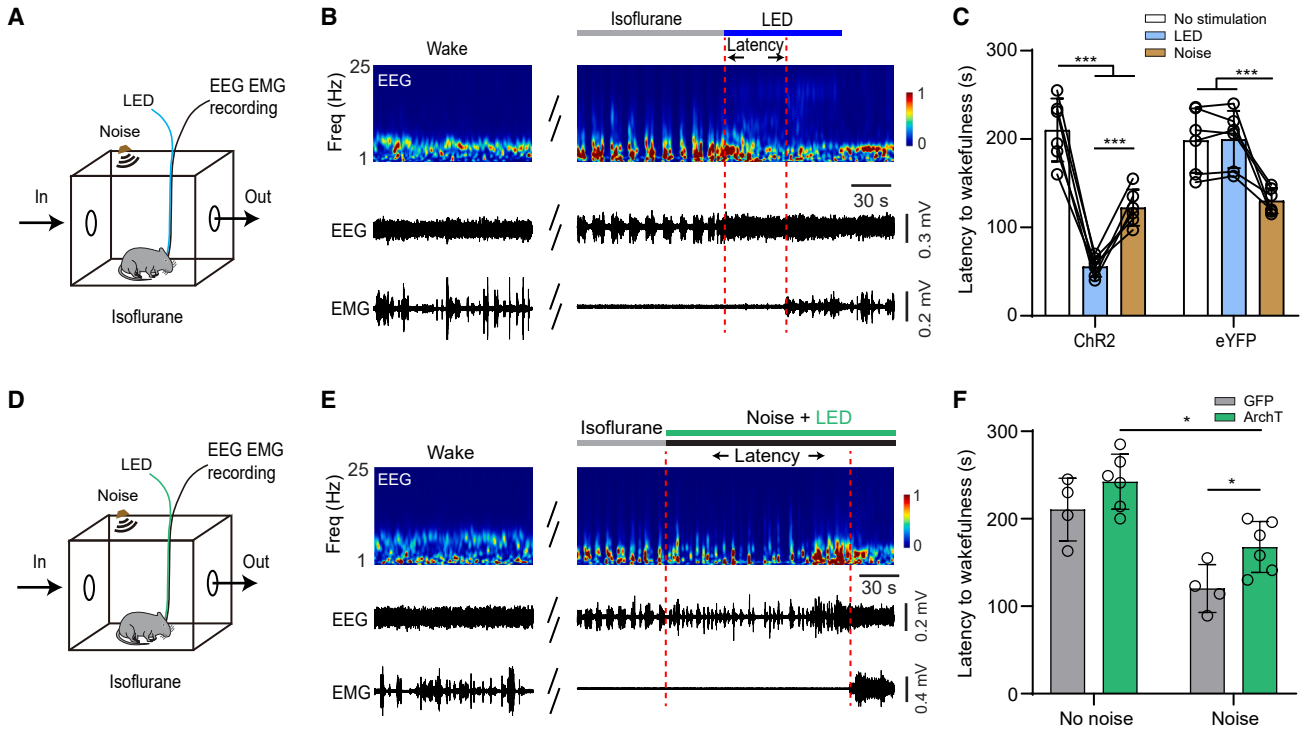

Figure 6. PCG glutamatergic neurons facilitate emergence from anesthesia

(A) Experimental condition: the mouse was anesthetized with isoflurane and optogenetic stimulation was applied to PCG glutamatergic neurons with simultaneous EEG/EMG recordings.

(B) Left: EEG power spectrum and EEG/EMG traces during wakefulness before anesthesia. Right: EEG power spectrum and EEG/EMG traces around the termination of anesthesia (gray horizontal bar) and onset of LED stimulation (blue horizontal bar). Dashed red vertical lines depict the latency to wakefulness.

(C) Latency to wakefulness from anesthesia in three conditions: no stimulation, with LED stimulation, and with noise stimulation. Data points for the same animal are connected with lines. ***$p < 0.001$, one-way ANOVA with Tukey's post hoc test, $n = 6$ mice for both ChR2 and eYFP groups.

(D) Experimental condition: optogenetic inhibition was applied to PCG glutamatergic neurons.

(E) Representative EEG power spectrum and EEG/EMG traces during wakefulness and around the termination of anesthesia and onset of sound stimulation coupled with optogenetic inhibition (green horizontal bar).

(F) Latency to wakefulness from anesthesia in two conditions: without noise stimulation and with noise stimulation (70 dB SPL). *$p < 0.05$, t test performed between ArchT and GFP groups; paired t test performed between two conditions for ArchT group; $n = 4$ and 6 mice for GFP and ArchT group, respectively. All error bars represent SD.

See also Figure S2.

Bilateral optical activation of PCG glutamatergic neurons was applied immediately after the termination of isoflurane anesthesia (Figure 6B). Compared with natural, spontaneous awakening from anesthesia, the optogenetic activation significantly shortened the latency to wakefulness, whereas this effect was absent in eYFP control mice (Figure 6C, white and blue). Thus, activation of PCG glutamatergic neurons greatly accelerated the emergence from anesthesia. Sensory stimulation with sustained auditory noise (at 70 dB SPL) also accelerated the emergence from anesthesia, but with lower effectiveness compared with the direct activation of PCG glutamatergic neurons (Figure 6C, brown).

We next examined whether PCG glutamatergic neurons could contribute to auditory-induced awakening from anesthesia by optogenetically inhibiting these neurons after expressing ArchT (Figure 6D). Sustained auditory noise was applied immediately after the termination of isoflurane anesthesia with green LED light simultaneously delivered (Figure 6E). Although the latency to wakefulness did not differ between ArchT-expressing and GFP control animals in the no-noise (spontaneous awakening) condition, it was significantly longer in ArchT-expressing than GFP control animals in the noise stimulation condition (Figure 6F). Our data are thus consistent with the notion that PCG glutamatergic neurons can also play a role in promoting auditory-induced awakening from anesthesia. Nevertheless, we do not exclude the possibility that these neurons can be more generally involved in arousal beyond sound-induced awakening.

PCG glutamatergic neurons promote wakefulness through specific downstream projections

Finally, we examined which of the downstream projections might play a role in the PCG-mediated promotion of wakefulness. To test this, we optically stimulated ChR2-expressing axon terminals from PCG glutamatergic neurons in each of the five target areas: MD, VTA, LHA, LPO, and PVT. To minimize confounds caused by potential backpropagation of action potentials,[43] we concurrently injected muscimol into PCG to silence its neuronal cell bodies (Figure 7A), following our previous study.[20] In this

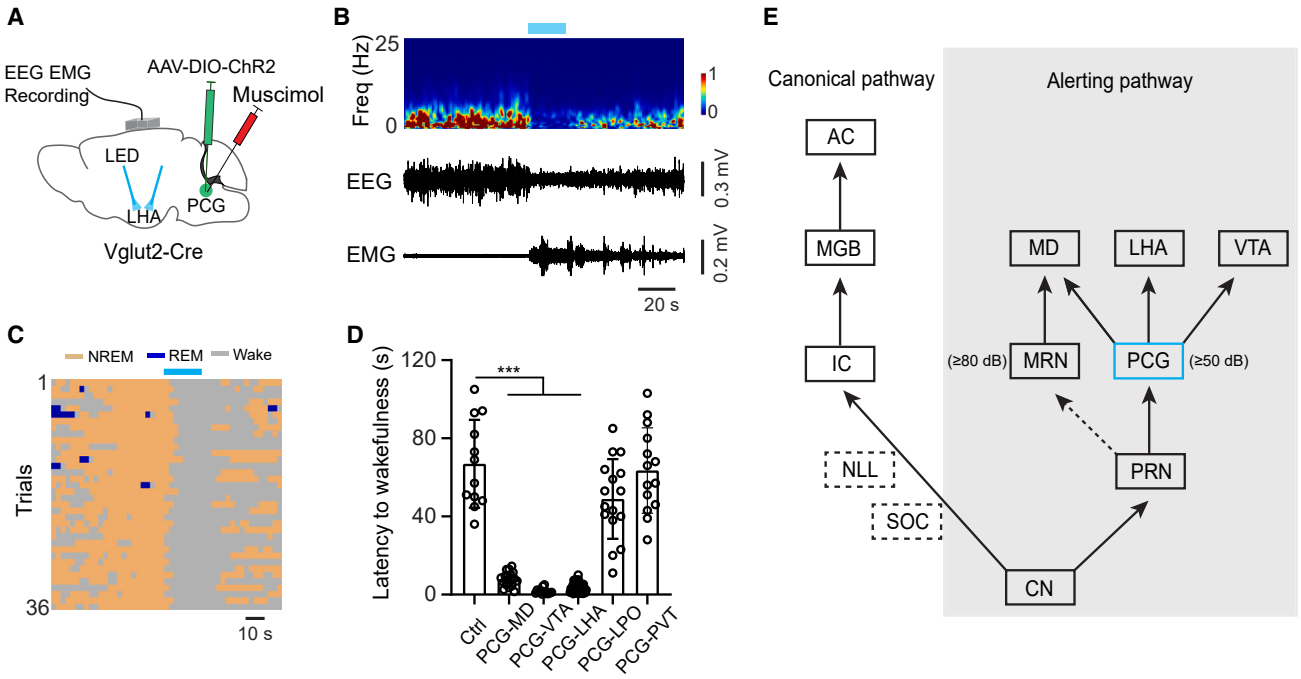

Figure 7. PCG glutamatergic neurons mediate awakening through specific downstream projections

(A) Schematic viral injection and optical stimulation of PCG-to-LHA terminals (bilateral). Muscimol was injected into PCG concurrently.

(B) EEG power spectrum (top) and EEG/EMG recording traces (bottom) for an example animal awakened from NREM sleep. Blue bar marks the optical stimulation.

(C) Sleep/wake states around the optical stimulation of the PCG-to-LHA projection (blue bar) in ChR2-expressing mice (n = 4 mice, 36 trials in total).

(D) Average latency to wakefulness induced by the terminal activation in different PCG targets. ***$p < 0.001$, one-way ANOVA with Tukey's post hoc test. Error bars represent SD.

(E) A working model for the PCG-mediated alerting pathway. PCG transmits bottom-up alerting sensory signals to MD, LHA, and VTA, thus activating the global arousal-related network. This results in rapid awakening from sleep upon external events. Note that MRN has a much higher intensity threshold than PCG while transmitting auditory signals to MD. SOC, superior olivary complex; MGB, medial geniculate body. Dash line represents unconfirmed pathway.

condition, bilateral stimulation of the PCG to MD, VTA, and LHA projections reliably elicited transitions to wakefulness from NREM sleep (Figures 7B–7D). By contrast, stimulation of the PCG projection to LPO or PVT failed to induce a transition from NREM sleep to wakefulness (Figure 7D), although the PVT has been shown to be a critical thalamic area for controlling wakefulness.[32] Together, although the backpropagation of action potentials cannot be completely ruled out, our data suggest that PCG glutamatergic neurons promote wakefulness primarily through their projections to the MD, LHA, and VTA.

DISCUSSION

In this study, we have demonstrated that a bottom-up brainstem auditory circuit unrelated to auditory perception contributes to sound-induced awakening (Figure 7E). As a central node in this circuit, the PCG can propagate alerting sound signals to a variety of downstream targets related to arousal. Using cell-type-specific approaches, we further demonstrated that the glutamatergic neurons in this structure play an important role in sound-induced awakening and sleep/wake transitions. Optogenetic activation of these neurons induces rapid transitions from sleep to wakefulness, whereas inhibition of them reduces the probability of auditory-induced awakening and increases the time in sleep during natural sleep-wake cycles. Our results suggest that the PCG serves as a critical hub to broadcast biologically salient auditory information to a global arousal-related network to mediate rapid awakening from sleep in response to external sensory events.

The PCG broadcasts auditory information to a global arousal-related network

The ability to rapidly wake up from sleep in response to auditory threats in a dangerous environment is critical for animal survival.[2,5–11] In an attempt to identify neuronal circuits that mediate sound-induced awakening, we have discovered that PCG, which is an important node of the noncanonical reticular-limbic auditory pathway,[18] plays a critical role in transmitting alerting sound signals. Although not responsive to tone stimuli, PCG neurons respond to noise sounds with a moderately high intensity threshold, consistent with the notion that they are involved in relaying information about not the auditory content but the valence of acoustic events.[20,25] Sensory stimuli that can wake animals typically have a valence value and evoke emotional arousal.[44] PCG projects axons to a multitude of brain regions involved in arousal, including the MD, PVT, LHA, VTA, LPO, and MS,[20] suggesting that it may be able to activate a global, distributed arousal system.

In this study, by comparing auditory noise responses in these different brain regions, we found that the auditory input to the MD, a thalamic area implicated in sound-driven awakening,[29] originates primarily from the PCG. Pharmacological silencing of PCG nearly abolishes the auditory response in each of these downstream areas except the VTA, confirming that the PCG broadcasts the alerting auditory signals to divergent targets. That PCG silencing only partially blocks the auditory response in the VTA (Figure 2F) suggests additional PCG-independent pathways to VTA, possibly via the striatum.[45–47] Based on the literature, nearly all these downstream areas are arousal related. For instance, optogenetic activation of glutamatergic neurons in the PVT induces wakefulness from NREM sleep through their projections to the nucleus accumbens.[32] Direct photostimulation of hypocretin/orexin neurons in the lateral hypothalamus[31] and glutamatergic or dopaminergic neurons in the VTA[33,34] also results in wakefulness from sleep. Meanwhile, calretinin+ neurons in the MD mediate distinct levels of forebrain arousal.[48] In agreement with these previous results, our data demonstrate that activation of PCG glutamatergic axons in the MD, LHA, and VTA directly promotes awakening (Figure 7D). However, activation of PCG axons in the PVT or LPO may not be sufficient for inducing sleep-to-wake transitions. Together, our results demonstrate that PCG, via its glutamatergic neurons, broadcasts bottom-up alerting auditory information to a global network of arousal-related structures and that these divergent PCG-mediated pathways may act synergistically to enhance arousal.

Our data show that in naive (without any particular training) conditions, MRN is unlikely a major input source for auditory responses in MD because MRN neurons exhibit extremely high intensity thresholds (around 80 dB SPL). This, however, does not exclude the possibility that, after reinforced learning, MRN neurons could gain responses to behaviorally relevant auditory cues.[30] In addition, it does not preclude a potential role of MRN in auditory-induced awakening under extremely loud sounds. The origin of auditory information for the MRN remains an open question. Recent studies have proposed IC and NLL, both of which directly receive inputs from the CN.[29,30] Our anatomical results indicate that MRN also receives some axonal projections from PCG[20] and that it is one major downstream target of PRN (data not shown). More studies are needed to determine more precisely the auditory input source of MRN.

PCG glutamatergic neurons mediate sound-induced awakening

In the mammalian central nervous system, several neurotransmitter/neuromodulatory systems are traditionally known to be involved in the regulation of sleep-wake transitions.[49–51] These include the noradrenergic neurons in the LC,[52,53] serotonergic neurons in the dorsal raphe nuclei (DRN),[54,55] dopaminergic neurons/projections mainly in the VTA and nucleus accumbens,[33,34] histaminergic neurons in the tuberomammillary nucleus,[56] orexinergic neurons in the lateral hypothalamus,[57] and cholinergic neurons in the basal forebrain and brainstem.[40,58,59] These systems, when artificially activated, generally promote waking from sleep in studies of intrinsic sleep/wake transitions.[7,13,34,53,60–62] However, the neural circuit mechanisms through which the external sensory stimuli affect sleep-wake states remain understudied.

Our present study highlights an essential role of PCG glutamatergic neurons in rapid awakening from sleep upon external acoustic events. Activating these neurons directly induces awakening from both NREM and REM sleep, in particular ultrafast awakening from NREM sleep, whereas inhibiting them significantly diminishes the probability of sound-induced awakening from NREM sleep. Although these findings are consistent with a direct role of PCG glutamatergic neurons in mediating the sound-induced awakening, it remains possible that these neurons are a critical component of a large, distributed network to support arousal in general beyond the sound-induced awakening. In addition, we have reported previously that PCG can respond to sensory stimuli of multiple modalities,[20,25] raising the possibility that this structure can play a role in arousal and awakening induced not only by acoustic events but also by those across different sensory modalities.

It is worth noting that inhibition of PCG glutamatergic neurons did not completely block auditory-induced awakening or sleep-to-wake transitions. This suggests the existence of other pathways. A recent study has identified the medial sector of the auditory thalamus (ATm), which includes the medial geniculate body and the posterior intralaminar nucleus, as a region mediating auditory-induced awakening.[63] This may constitute a separate pathway from the one identified in our present study because the MD thalamus, a major downstream target of PCG, is distinct from the ATm. Additionally, the activity of noradrenergic neurons in the LC has been shown to regulate the threshold of sensory-evoked awakening[12] and that of dopaminergic neurons in the DRN is correlated with the probability of sensory-evoked awakening.[13] These structures likely also contribute to sound-induced awakening. It is also worth mentioning that inhibition of PCG glutamatergic neurons did not appear to affect sound-induced awakening from REM sleep (Figure 4C). Similar to our result, recent studies have shown that optogenetic inhibition of noradrenergic activity in the LC[12] or dopamine neurons in the DRN[13] does not affect awakening from REM sleep. These findings suggest that REM and NREM sleep could be mechanistically different.

Our previous study[20] has suggested that PCG glutamatergic neurons receive higher-structure inputs mainly from midbrain structures, including the interpeduncular nucleus (IPN), periaqueductal gray, superior colliculus, and MRN, all of which have been implicated in sleep/wake regulation.[29,64–66] In addition, they receive limited cortical input from the retrosplenial cortex (RSP).[20] These suggest potential top-down regulations of the PCG function in the sleep/wake control. For example, the IPN is involved in mood regulation[67,68] and may integrate sensory and internal-state signals to modulate the excitability of PCG neurons. The RSP, involved in higher-level cognitive functions, may modulate PCG activity based on contextual and cognitive factors.[69]

A fast-execution alerting system via PCG

Apart from the circadian regulation of sleep, a fast-execution alerting system is required to rapidly wake animals from sleep in response to imminent threats, such as approaching predators.[5,8–10,70] Whether there are specific brain structures devoted to this function has not been clear. In the present study, we found that the PCG-mediated awakening from NREM sleep is sub-second, with much shorter latencies to wakefulness (~100 ms on

average) than those reported for other systems. For instance, latency to wakefulness has been reported to be ~20–30 s for hypocretin/orexin neurons[31] or ~1–5 s for neurotensin neurons[71] in the lateral hypothalamus, ~4 s for norepinephrine neurons in the LC,[53] ~5–15 s for cholinergic neurons[58,72] or ~3–5 s for PV neurons[10] in the basal forebrain, ~2 s for dopamine neurons in the VTA,[34] and ~1.7 s for neurons in the ATm.[63] The ultra-fast awakening by activating PCG suggests a reliance on fast neurotransmission rather than slower neuromodulatory effects, as well as on feedforward rather than feedback circuits. Consistent with a bottom-up nature of sensory relay,[18] the PCG responds rapidly to auditory stimuli, with a latency as short as 7 ms (Figure 1I). As such, it is strategically positioned to function within a rapidly responding alerting system, allowing animals to react immediately to imminent threats even during sleep. The enhanced sensory responses of PCG glutamatergic neurons during sleep relative to wakefulness (Figures 5K and 5L), which suggests heightened sensitivity to external events, may further facilitate such a functional role. Activating one PCG target, MD,[29] or another thalamic area, the centromedial thalamus,[73] also results in awakening with longer latencies (in seconds). This further suggests that potentially synergistic actions of multiple PCG downstream targets can ensure the extremely fast wake-promoting effect.

PCG glutamatergic activity modulates intrinsic sleep/wake cycles

In addition to sensory-induced awakening, we discovered that the function of PCG glutamatergic neurons is also linked to the intrinsic states of vigilance: their overall activity level is highest during wakefulness and lowest during NREM sleep. Changes in their baseline firing rate are associated with spontaneous transitions between sleep/wake states. Moreover, inhibition of these neurons reduces wakefulness and prolongs the time in NREM sleep. These data demonstrate that the activity of PCG glutamatergic neurons can modulate natural sleep-wake cycles and highlight their potential role in maintaining the baseline arousal state. Thus, these PCG neurons can generally promote wakefulness.

In summary, our study elucidates an important role of PCG in transmitting alerting auditory signals to a global arousal-related brain network and its critical role in mediating fast sound-induced awakening from sleep. Through this PCG-mediated ascending alerting system (Figure 7E), external sensory events can rapidly impact on arousal and internally regulated sleep.

RESOURCE AVAILABILITY

Lead contact

Further information and requests for resources and reagents should be directed to and will be fulfilled by the lead contact, Li I. Zhang (liizhang@usc.edu).

Materials availability

This study did not generate new unique reagents.

Data and code availability

- All data reported in this paper will be shared by the lead contact upon reasonable request.
- All original code has been deposited at Zenodo and is publicly available as of the date of publication. DOIs are listed in the key resources table.
- Any additional information required to reanalyze the data reported in this paper is available upon request.

ACKNOWLEDGMENTS

This work was supported by grants from the US National Institutes of Health (R01DC008983, RF1MH114112, and MH116990 to L.I.Z.; EY019049 and MH116990 to H.W.T.).

AUTHOR CONTRIBUTIONS

L.I.Z. and H.W.T. conceived the study and supervised the project. J.W. and C.X. carried out anatomical, *in vivo* recording and all behavioral experiments as well as data analysis. G.-W.Z. contributed to experiments on sleep recordings. L.S. contributed to data analysis for sleep experiments. C.X., L.I.Z., and H.W.T. wrote the manuscript.

DECLARATION OF INTERESTS

The authors declare no competing interests.

STAR★METHODS

Detailed methods are provided in the online version of this paper and include the following:

- KEY RESOURCES TABLE
- EXPERIMENTAL MODEL AND SUBJECT DETAILS
- METHOD DETAILS
  - Viral injection
  - Optogenetic manipulation
  - Awake head-fixed animal preparation
  - Sound generation and stimuli
  - EEG and EMG electrodes implantation
  - EEG/EMG data acquisition, processing, and sleep-wake state classification
  - Anesthesia experiments
  - Pharmacological silencing
  - Chemogenetic silencing
  - *In vivo* multichannel electrophysiological recordings
  - Fiber photometry recording and data analysis
  - TRAP induction
  - Histology, imaging and quantification
- QUANTIFICATION AND STATISTICAL ANALYSIS
  - Data analysis
  - Statistics

SUPPLEMENTAL INFORMATION

Supplemental information can be found online at https://doi.org/10.1016/j.cub.2024.08.020.

Received: March 11, 2024
Revised: July 12, 2024
Accepted: August 13, 2024
Published: September 11, 2024

REFERENCES

1. Steriade, M. (2005). Brain electrical activity and sensory processing during waking and sleep states. In Principles and Practice of Sleep Medicine (Elsevier), pp. 101–119. https://doi.org/10.1016/B0-72-160797-7/50016-1.
2. Halász, P., Terzano, M., Parrino, L., and Bódizs, R. (2004). The nature of arousal in sleep. J. Sleep Res. *13*, 1–23. https://doi.org/10.1111/j.1365-2869.2004.00388.x.
3. Anafi, R.C., Kayser, M.S., and Raizen, D.M. (2019). Exploring phylogeny to find the function of sleep. Nat. Rev. Neurosci. *20*, 109–116. https://doi.org/10.1038/s41583-018-0098-9.

4. Campbell, S.S., and Tobler, I. (1984). Animal sleep: a review of sleep duration across phylogeny. Neurosci. Biobehav. Rev. *8*, 269–300. https://doi.org/10.1016/0149-7634(84)90054-x.

5. Velluti, R.A. (1997). Interactions between sleep and sensory physiology. J. Sleep Res. *6*, 61–77. https://doi.org/10.1046/j.1365-2869.1997.00031.x.

6. Kaur, S., Pedersen, N.P., Yokota, S., Hur, E.E., Fuller, P.M., Lazarus, M., Chamberlin, N.L., and Saper, C.B. (2013). Glutamatergic signaling from the parabrachial nucleus plays a critical role in hypercapnic arousal. J. Neurosci. *33*, 7627–7640. https://doi.org/10.1523/JNEUROSCI.0173-13.2013.

7. Kaur, S., De Luca, R., Khanday, M.A., Bandaru, S.S., Thomas, R.C., Broadhurst, R.Y., Venner, A., Todd, W.D., Fuller, P.M., Arrigoni, E., and Saper, C.B. (2020). Role of serotonergic dorsal raphe neurons in hypercapnia-induced arousals. Nat. Commun. *11*, 2769. https://doi.org/10.1038/s41467-020-16518-9.

8. Campos, C.A., Bowen, A.J., Roman, C.W., and Palmiter, R.D. (2018). Encoding of danger by parabrachial CGRP neurons. Nature *555*, 617–622. https://doi.org/10.1038/nature25511.

9. Browne, L.E., Latremoliere, A., Lehnert, B.P., Grantham, A., Ward, C., Alexandre, C., Costigan, M., Michoud, F., Roberson, D.P., Ginty, D.D., and Woolf, C.J. (2017). Time-resolved fast mammalian behavior reveals the complexity of protective pain responses. Cell Rep. *20*, 89–98. https://doi.org/10.1016/j.celrep.2017.06.024.

10. McKenna, J.T., Thankachan, S., Uygun, D.S., Shukla, C., McNally, J.M., Schiffino, F.L., Cordeira, J., Katsuki, F., Zant, J.C., Gamble, M.C., et al. (2020). Basal forebrain parvalbumin neurons mediate arousals from sleep induced by hypercarbia or auditory stimuli. Curr. Biol. *30*, 2379–2385.e4. https://doi.org/10.1016/j.cub.2020.04.029.

11. Wang, X., Chou, X.-L., Zhang, L.I., and Tao, H.W. (2020). Zona incerta: an integrative node for global behavioral modulation. Trends Neurosci. *43*, 82–87. https://doi.org/10.1016/j.tins.2019.11.007.

12. Hayat, H., Regev, N., Matosevich, N., Sales, A., Paredes-Rodriguez, E., Krom, A.J., Bergman, L., Li, Y., Lavigne, M., Kremer, E.J., et al. (2020). Locus coeruleus norepinephrine activity mediates sensory-evoked awakenings from sleep. Sci. Adv. *6*, eaaz4232. https://doi.org/10.1126/sciadv.aaz4232.

13. Cho, J.R., Treweek, J.B., Robinson, J.E., Xiao, C., Bremner, L.R., Greenbaum, A., and Gradinaru, V. (2017). Dorsal raphe dopamine neurons modulate arousal and promote wakefulness by salient stimuli. Neuron *94*, 1205–1219.e8. https://doi.org/10.1016/j.neuron.2017.05.020.

14. Garey, J., Goodwillie, A., Frohlich, J., Morgan, M., Gustafsson, J.A., Smithies, O., Korach, K.S., Ogawa, S., and Pfaff, D.W. (2003). Genetic contributions to generalized arousal of brain and behavior. Proc. Natl. Acad. Sci. USA *100*, 11019–11022. https://doi.org/10.1073/pnas.1633773100.

15. Neckelmann, D., and Ursin, R. (1993). Sleep stages and EEG power spectrum in relation to acoustical stimulus arousal threshold in the rat. Sleep *16*, 467–477. https://doi.org/10.1093/sleep/16.5.467.

16. Bonnet, M.H., and Moore, S.E. (1982). The threshold of sleep: perception of sleep as a function of time asleep and auditory threshold. Sleep *5*, 267–276. https://doi.org/10.1093/sleep/5.3.267.

17. Wu, G.K., Tao, H.W., and Zhang, L.I. (2011). From elementary synaptic circuits to information processing in primary auditory cortex. Neurosci. Biobehav. Rev. *35*, 2094–2104. https://doi.org/10.1016/j.neubiorev.2011.05.004.

18. Zhang, G.W., Sun, W.J., Zingg, B., Shen, L., He, J., Xiong, Y., Tao, H.W., and Zhang, L.I. (2018). A non-canonical reticular-limbic central auditory pathway via medial septum contributes to fear conditioning. Neuron *97*, 406–417.e4. https://doi.org/10.1016/j.neuron.2017.12.010.

19. Billig, A.J., Lad, M., Sedley, W., and Griffiths, T.D. (2022). The hearing hippocampus. Prog. Neurobiol. *218*, 102326. https://doi.org/10.1016/j.pneurobio.2022.102326.

20. Xiao, C., Wei, J., Zhang, G.W., Tao, C., Huang, J.J., Shen, L., Wickersham, I.R., Tao, H.W., and Zhang, L.I. (2023). Glutamatergic and GABAergic neurons in pontine central gray mediate opposing valence-specific behaviors through a global network. Neuron *111*, 1486–1503.e7. https://doi.org/10.1016/j.neuron.2023.02.012.

21. Edlow, B.L., Takahashi, E., Wu, O., Benner, T., Dai, G., Bu, L., Grant, P.E., Greer, D.M., Greenberg, S.M., Kinney, H.C., and Folkerth, R.D. (2012). Neuroanatomic connectivity of the human ascending arousal system critical to consciousness and its disorders. J. Neuropathol. Exp. Neurol. *71*, 531–546. https://doi.org/10.1097/NEN.0b013e3182588293.

22. Moruzzi, G., and Magoun, H.W. (1949). Brain stem reticular formation and activation of the EEG. Electroencephalogr. Clin. Neurophysiol. *1*, 455–473. https://doi.org/10.1016/0013-4694(49)90219-9.

23. Young, G.B. (2009). Coma. Ann. N. Y. Acad. Sci. *1157*, 32–47. https://doi.org/10.1111/j.1749-6632.2009.04471.x.

24. Fuller, P.M., Sherman, D., Pedersen, N.P., Saper, C.B., and Lu, J. (2011). Reassessment of the structural basis of the ascending arousal system. J. Comp. Neurol. *519*, 933–956. https://doi.org/10.1002/cne.22559.

25. Zhang, G.W., Shen, L., Zhong, W., Xiong, Y., Zhang, L.I., and Tao, H.W. (2018). Transforming sensory cues into aversive emotion via septal-habenular pathway. Neuron *99*, 1016–1028.e5. https://doi.org/10.1016/j.neuron.2018.07.023.

26. Takeuchi, Y., Nagy, A.J., Barcsai, L., Li, Q., Ohsawa, M., Mizuseki, K., and Berényi, A. (2021). The medial septum as a potential target for treating brain disorders associated with oscillopathies. Front. Neural Circuits *15*, 701080. https://doi.org/10.3389/fncir.2021.701080.

27. Fuhrmann, F., Justus, D., Sosulina, L., Kaneko, H., Beutel, T., Friedrichs, D., Schoch, S., Schwarz, M.K., Fuhrmann, M., and Remy, S. (2015). Locomotion, theta oscillations, and the speed-correlated firing of hippocampal neurons are controlled by a medial septal glutamatergic circuit. Neuron *86*, 1253–1264. https://doi.org/10.1016/j.neuron.2015.05.001.

28. Lu, L., Ren, Y., Yu, T., Liu, Z., Wang, S., Tan, L., Zeng, J., Feng, Q., Lin, R., Liu, Y., et al. (2020). Control of locomotor speed, arousal, and hippocampal theta rhythms by the nucleus incertus. Nat. Commun. *11*, 262. https://doi.org/10.1038/s41467-019-14116-y.

29. Shin, A., Park, S., Shin, W., Woo, J., Jeong, M., Kim, J., and Kim, D. (2023). A brainstem-to-mediodorsal thalamic pathway mediates sound-induced arousal from slow-wave sleep. Curr. Biol. *33*, 875–885.e5. https://doi.org/10.1016/j.cub.2023.01.033.

30. Inagaki, H.K., Chen, S., Ridder, M.C., Sah, P., Li, N., Yang, Z., Hasanbegovic, H., Gao, Z., Gerfen, C.R., and Svoboda, K. (2022). A midbrain-thalamus-cortex circuit reorganizes cortical dynamics to initiate movement. Cell *185*, 1065–1081.e23. https://doi.org/10.1016/j.cell.2022.02.006.

31. Adamantidis, A.R., Zhang, F., Aravanis, A.M., Deisseroth, K., and De Lecea, L. (2007). Neural substrates of awakening probed with optogenetic control of hypocretin neurons. Nature *450*, 420–424. https://doi.org/10.1038/nature06310.

32. Ren, S., Wang, Y., Yue, F., Cheng, X., Dang, R., Qiao, Q., Sun, X., Li, X., Jiang, Q., Yao, J., et al. (2018). The paraventricular thalamus is a critical thalamic area for wakefulness. Science *362*, 429–434. https://doi.org/10.1126/science.aat2512.

33. Yu, X., Li, W., Ma, Y., Tossell, K., Harris, J.J., Harding, E.C., Ba, W., Miracca, G., Wang, D., Li, L., et al. (2019). GABA and glutamate neurons in the VTA regulate sleep and wakefulness. Nat. Neurosci. *22*, 106–119. https://doi.org/10.1038/s41593-018-0288-9.

34. Eban-Rothschild, A., Rothschild, G., Giardino, W.J., Jones, J.R., and De Lecea, L. (2016). VTA dopaminergic neurons regulate ethologically relevant sleep-wake behaviors. Nat. Neurosci. *19*, 1356–1366. https://doi.org/10.1038/nn.4377.

35. Yamagata, T., Kahn, M.C., Prius-Mengual, J., Meijer, E., Šabanović, M., Guillaumin, M.C.C., van der Vinne, V., Huang, Y.G., McKillop, L.E., Jagannath, A., et al. (2021). The hypothalamic link between arousal and sleep homeostasis in mice. Proc. Natl. Acad. Sci. USA *118*, 1–12. https://doi.org/10.1073/pnas.2101580118.

36. Allen, W.E., DeNardo, L.A., Chen, M.Z., Liu, C.D., Loh, K.M., Fenno, L.E., Ramakrishnan, C., Deisseroth, K., and Luo, L. (2017). Thirst-associated preoptic neurons encode an aversive motivational drive. Science *357*, 1149–1155. https://doi.org/10.1126/science.aan6747.

37. DeNardo, L.A., Liu, C.D., Allen, W.E., Adams, E.L., Friedmann, D., Fu, L., Guenthner, C.J., Tessier-Lavigne, M., and Luo, L. (2019). Temporal evolution of cortical ensembles promoting remote memory retrieval. Nat. Neurosci. *22*, 460–469. https://doi.org/10.1038/s41593-018-0318-7.

38. Guenthner, C.J., Miyamichi, K., Yang, H.H., Heller, H.C., and Luo, L. (2013). Permanent genetic access to transiently active neurons via TRAP: Targeted recombination in active populations. Neuron *78*, 773–784. https://doi.org/10.1016/j.neuron.2013.03.025.

39. Cox, J., Pinto, L., and Dan, Y. (2016). Calcium imaging of sleep-wake related neuronal activity in the dorsal pons. Nat. Commun. *7*, 10763. https://doi.org/10.1038/ncomms10763.

40. Boucetta, S., Cissé, Y., Mainville, L., Morales, M., and Jones, B.E. (2014). Discharge profiles across the sleep-waking cycle of identified cholinergic, GABAergic, and glutamatergic neurons in the pontomesencephalic tegmentum of the rat. J. Neurosci. *34*, 4708–4727. https://doi.org/10.1523/JNEUROSCI.2617-13.2014.

41. Tao, C., Zhang, G.-W., Huang, J.J., Li, Z., Tao, H.W., and Zhang, L.I. (2023). The medial preoptic area mediates depressive-like behaviors induced by ovarian hormone withdrawal through distinct GABAergic projections. Nat. Neurosci. *26*, 1529–1540. https://doi.org/10.1038/s41593-023-01397-2.

42. Wang, X., Chou, X., Peng, B., Shen, L., Huang, J.J., Zhang, L.I., and Tao, H.W. (2019). A cross-modality enhancement of defensive flight via parvalbumin neurons in zonal incerta. eLife *8*, 1–17. https://doi.org/10.7554/eLife.42728.

43. Mitani, K., Kawabata, M., Isomura, Y., and Sakai, Y. (2022). Automated and parallelized spike collision tests to identify spike signal projections. iScience *25*, 105071. https://doi.org/10.1016/j.isci.2022.105071.

44. Namburi, P., Al-Hasani, R., Calhoon, G.G., Bruchas, M.R., and Tye, K.M. (2016). Architectural representation of valence in the limbic system. Neuropsychopharmacology *41*, 1697–1715. https://doi.org/10.1038/npp.2015.358.

45. Guo, L., Walker, W.I., Ponvert, N.D., Penix, P.L., and Jaramillo, S. (2018). Stable representation of sounds in the posterior striatum during flexible auditory decisions. Nat. Commun. *9*, 1534. https://doi.org/10.1038/s41467-018-03994-3.

46. Chen, L., Wang, X., Ge, S., and Xiong, Q. (2019). Medial geniculate body and primary auditory cortex differentially contribute to striatal sound representations. Nat. Commun. *10*, 418. https://doi.org/10.1038/s41467-019-08350-7.

47. Beier, K.T., Gao, X.J., Xie, S., DeLoach, K.E., Malenka, R.C., and Luo, L. (2019). Topological organization of ventral tegmental area connectivity revealed by viral-genetic dissection of input-output relations. Cell Rep. *26*, 159–167.e6. https://doi.org/10.1016/j.celrep.2018.12.040.

48. Mátyás, F., Komlósi, G., Babiczky, Á., Kocsis, K., Barthó, P., Barsy, B., Dávid, C., Kanti, V., Porrero, C., Magyar, A., et al. (2018). A highly collateralized thalamic cell type with arousal-predicting activity serves as a key hub for graded state transitions in the forebrain. Nat. Neurosci. *21*, 1551–1562. https://doi.org/10.1038/s41593-018-0251-9.

49. Scammell, T.E., Arrigoni, E., and Lipton, J.O. (2017). Neural circuitry of wakefulness and sleep. Neuron *93*, 747–765. https://doi.org/10.1016/j.neuron.2017.01.014.

50. Liu, D., and Dan, Y. (2019). A motor theory of sleep-wake control: arousal-action circuit. Annu. Rev. Neurosci. *42*, 27–46. https://doi.org/10.1146/annurev-neuro-080317-061813.

51. Brown, R.E., Basheer, R., McKenna, J.T., Strecker, R.E., and McCarley, R.W. (2012). Control of sleep and wakefulness. Physiol. Rev. *92*, 1087–1187. https://doi.org/10.1152/physrev.00032.2011.

52. Aston-Jones, G., and Cohen, J.D. (2005). An integrative theory of locus coeruleus-norepinephrine function: adaptive gain and optimal performance. Annu. Rev. Neurosci. *28*, 403–450. https://doi.org/10.1146/annurev.neuro.28.061604.135709.

53. Carter, M.E., Yizhar, O., Chikahisa, S., Nguyen, H., Adamantidis, A., Nishino, S., Deisseroth, K., and De Lecea, L. (2010). Tuning arousal with optogenetic modulation of locus coeruleus neurons. Nat. Neurosci. *13*, 1526–1533. https://doi.org/10.1038/nn.2682.

54. Buchanan, G.F., and Richerson, G.B. (2010). Central serotonin neurons are required for arousal to CO2. Proc. Natl. Acad. Sci. USA *107*, 16354–16359. https://doi.org/10.1073/pnas.1004587107.

55. Saper, C.B., Chou, T.C., and Scammell, T.E. (2001). The sleep switch: Hypothalamic control of sleep and wakefulness. Trends Neurosci. *24*, 726–731. https://doi.org/10.1016/S0166-2236(00)02002-6.

56. Parmentier, R., Ohtsu, H., Djebbara-Hannas, Z., Valatx, J.L., Watanabe, T., and Lin, J.S. (2002). Anatomical, physiological, and pharmacological characteristics of histidine decarboxylase knock-out mice: Evidence for the role of brain histamine in behavioral and sleep-wake control. J. Neurosci. *22*, 7695–7711. https://doi.org/10.1523/JNEUROSCI.22-17-07695.2002.

57. Herrera, C.G., Cadavieco, M.C., Jego, S., Ponomarenko, A., Korotkova, T., and Adamantidis, A. (2016). Hypothalamic feedforward inhibition of thalamocortical network controls arousal and consciousness. Nat. Neurosci. *19*, 290–298. https://doi.org/10.1038/nn.4209.

58. Han, Y., Shi, Y.F., Xi, W., Zhou, R., Tan, Z.B., Wang, H., Li, X.M., Chen, Z., Feng, G., Luo, M., et al. (2014). Selective activation of cholinergic basal forebrain neurons induces immediate sleep-wake transitions. Curr. Biol. *24*, 693–698. https://doi.org/10.1016/j.cub.2014.02.011.

59. Xu, M., and Dan, Y. (2015). Basal forebrain circuit for brain state control. Nat. Neurosci. *18*, 1641–1647.

60. Breton-Provencher, V., and Sur, M. (2019). Active control of arousal by a locus coeruleus GABAergic circuit. Nat. Neurosci. *22*, 218–228. https://doi.org/10.1038/s41593-018-0305-z.

61. Yamaguchi, H., Hopf, F.W., Li, S.B., and de Lecea, L. (2018). In vivo cell type-specific CRISPR knockdown of dopamine beta hydroxylase reduces locus coeruleus evoked wakefulness. Nat. Commun. *9*, 5211. https://doi.org/10.1038/s41467-018-07566-3.

62. Luo, Y.J., Li, Y.D., Wang, L., Yang, S.R., Yuan, X.S., Wang, J., Cherasse, Y., Lazarus, M., Chen, J.F., Qu, W.M., and Huang, Z.L. (2018). Nucleus accumbens controls wakefulness by a subpopulation of neurons expressing dopamine D1 receptors. Nat. Commun. *9*, 1576. https://doi.org/10.1038/s41467-018-03889-3.

63. Wang, Y., You, L., Tan, K.M., Li, M., Zou, J., Zhao, Z., Hu, W., Li, T., Xie, F., Li, C., et al. (2023). A common thalamic hub for general and defensive arousal control. Neuron *111*, 3270–3287.e8. https://doi.org/10.1016/j.neuron.2023.07.007.

64. Funato, H., Sato, M., Sinton, C.M., Gautron, L., Williams, S.C., Skach, A., Elmquist, J.K., Skoultchi, A.I., and Yanagisawa, M. (2010). Loss of Goosecoid-like and DiGeorge syndrome critical region 14 in interpeduncular nucleus results in altered regulation of rapid eye movement sleep. Proc. Natl. Acad. Sci. USA *107*, 18155–18160. https://doi.org/10.1073/pnas.1012764107.

65. Weber, F., Hoang Do, J.P., Chung, S., Beier, K.T., Bikov, M., Saffari Doost, M., and Dan, Y. (2018). Regulation of REM and non-REM sleep by periaqueductal GABAergic neurons. Nat. Commun. *9*, 354. https://doi.org/10.1038/s41467-017-02765-w.

66. Miller, A.M., Obermeyer, W.H., Behan, M., and Benca, R.M. (1998). The superior colliculus-pretectum mediates the direct effects of light on sleep. Proc. Natl. Acad. Sci. USA *95*, 8957–8962. https://doi.org/10.1073/pnas.95.15.8957.

67. McLaughlin, I., Dani, J.A., and De Biasi, M. (2017). The medial habenula and interpeduncular nucleus circuitry is critical in addiction, anxiety, and mood regulation. J. Neurochem. *142*, 130–143. https://doi.org/10.1111/jnc.14008.

68. Wills, L., Ables, J.L., Braunscheidel, K.M., Caligiuri, S.P.B., Elayouby, K.S., Fillinger, C., Ishikawa, M., Moen, J.K., and Kenny, P.J. (2022).

Neurobiological mechanisms of nicotine reward and aversion. Pharmacol. Rev. *74*, 271–310. https://doi.org/10.1124/pharmrev.121.000299.

69. Mitchell, A.S., Czajkowski, R., Zhang, N., Jeffery, K., and Nelson, A.J.D. (2018). Retrosplenial cortex and its role in spatial cognition. Brain Neurosci. Adv. *2*, 2398212818757098. https://doi.org/10.1177/2398212818757098.
70. Kaur, S., Wang, J.L., Ferrari, L., Thankachan, S., Kroeger, D., Venner, A., Lazarus, M., Wellman, A., Arrigoni, E., Fuller, P.M., and Saper, C.B. (2017). A genetically defined circuit for arousal from sleep during hypercapnia. Neuron *96*, 1153–1167.e5. https://doi.org/10.1016/j.neuron.2017.10.009.
71. Naganuma, F., Kroeger, D., Bandaru, S.S., Absi, G., Madara, J.C., and Vetrivelan, R. (2019). Lateral hypothalamic neurotensin neurons promote arousal and hyperthermia. PLoS Biol. *17*, e3000172. https://doi.org/10.1371/journal.pbio.3000172.
72. Zant, J.C., Kim, T., Prokai, L., Szarka, S., McNally, J., McKenna, J.T., Shukla, C., Yang, C., Kalinchuk, A.V., McCarley, R.W., et al. (2016). Cholinergic neurons in the basal forebrain promote wakefulness by actions on neighboring non-cholinergic neurons: An opto-dialysis study. J. Neurosci. *36*, 2057–2067. https://doi.org/10.1523/JNEUROSCI.3318-15.2016.
73. Gent, T.C., Bandarabadi, M., Herrera, C.G., and Adamantidis, A.R. (2018). Thalamic dual control of sleep and wakefulness. Nat. Neurosci. *21*, 974–984. https://doi.org/10.1038/s41593-018-0164-7.
74. Zingg, B., Peng, B., Huang, J., Tao, H.W., and Zhang, L.I. (2020). Synaptic specificity and application of anterograde transsynaptic AAV for probing neural circuitry. J. Neurosci. *40*, 3250–3267. https://doi.org/10.1523/JNEUROSCI.2158-19.2020.
75. Zingg, B., Chou, X.-L., Zhang, Z.-G., Mesik, L., Liang, F., Tao, H.W., and Zhang, L.I. (2017). AAV-mediated anterograde transsynaptic tagging: mapping corticocollicular input-defined neural pathways for defense behaviors. Neuron *93*, 33–47. https://doi.org/10.1016/j.neuron.2016.11.045.
76. Fang, Q., Chou, X.-L., Peng, B., Zhong, W., Zhang, L.I., and Tao, H.W. (2020). A differential circuit via retino-colliculo-pulvinar pathway enhances feature selectivity in visual cortex through surround suppression. Neuron *105*, 355–369.e6. https://doi.org/10.1016/j.neuron.2019.10.027.
77. Shen, L., Zhang, G.-W., Tao, C., Seo, M.B., Zhang, N.K., Huang, J.J., Zhang, L.I., and Tao, H.W. (2022). A bottom-up reward pathway mediated by somatostatin neurons in the medial septum complex underlying appetitive learning. Nat. Commun. *13*, 1194. https://doi.org/10.1038/s41467-022-28854-z.
78. Teng, S., Zhen, F., Wang, L., Schalchli, J.C., Simko, J., Chen, X., Jin, H., Makinson, C.D., and Peng, Y. (2022). Control of non-REM sleep by ventrolateral medulla glutamatergic neurons projecting to the preoptic area. Nat. Commun. *13*, 4748. https://doi.org/10.1038/s41467-022-32461-3.
79. Zhong, P., Zhang, Z., Barger, Z., Ma, C., Liu, D., Ding, X., and Dan, Y. (2019). Control of non-REM sleep by midbrain neurotensinergic neurons. Neuron *104*, 795–809.e6. https://doi.org/10.1016/j.neuron.2019.08.026.
80. Costa-Miserachs, D., Portell-Cortés, I., Torras-Garcia, M., and Morgado-Bernal, I. (2003). Automated sleep staging in rat with a standard spreadsheet. J. Neurosci. Methods *130*, 93–101. https://doi.org/10.1016/s0165-0270(03)00229-2.
81. Tasaka, G.-I., Feigin, L., Maor, I., Groysman, M., DeNardo, L.A., Schiavo, J.K., Froemke, R.C., Luo, L., and Mizrahi, A. (2020). The temporal association cortex plays a key role in auditory-driven maternal plasticity. Neuron *107*, 566–579.e7. https://doi.org/10.1016/j.neuron.2020.05.004.

STAR★METHODS

KEY RESOURCES TABLE

REAGENT or RESOURCE	SOURCE	IDENTIFIER
Antibodies		
Fluorescent Nissl Stain	Invitrogen	RRID: AB_2572212
Bacterial and virus strains		
AAV1-CAG-FLEX-GFP-WPRE	A gift from Hongkui Zeng	Addgene viral prep # 51502-AAV1
AAV1-EF1a-DIO-hChR2-eYFP	A gift from Karl Deisseroth	Addgene viral prep # 20298-AAV1
AAV1-EF1a-DIO-eYFP	A gift from Karl Deisseroth	Addgene viral prep # 27056-AAV1
AAV1-CAG-FLEX-ArchT-GFP	A gift from Edward Boyden	Addgene viral prep # 29777-AAV1
AAV1-Syn-FLEX-GCamp6s-WPRE-SV4	A gift from Douglas Kim & GENIE Project	Addgene viral prep # 100845-AAV1
pAAV-EF1a-DIO-hM4D (Gi)-mCherry	A gift from Bryan Roth	Addgene viral prep # 50461
pAAV- EF1α-DIO-mCherry	A gift from Bryan Roth	Addgene viral prep # 50462
Chemicals, peptides, and recombinant proteins		
DiI	Invitrogen	D282
Muscimol, BODIPY TMR-X Conjugate	Invitrogen	M23400
Clozapine-N-oxide	Tocris	34233-69-7
Experimental models: Organisms/strains		
Mouse: C57BL/6J	The Jackson Laboratory	RRID: IMSR_JAX:000664
Mouse: VGluT2-ires-Cre mice	The Jackson Laboratory	RRID: IMSR_JAX: 016963
Mouse: Fos$^{2A\text{-}iCreERT2}$ (TRAP2)	The Jackson Laboratory	RRID: IMSR_JAX: 030323
Mouse: Ai14	The Jackson Laboratory	RRID: IMSR_JAX: 007914
Software and algorithms		
Data acquisition with Labview	LabVIEW	http://www.ni.com/en-us/shop/labview.html; RRID: SCR_014325
Custom-written MATLAB code for analysis	MATLAB	http://www.mathworks.com/; RRID: SCR_001622
Allen Reference Atlas	McLaughlin et al.[67]	http://www.brainmap.org/; RRID: RRID: SCR_008848
Offline sorter	Plexon	http://plexon.com/; RRID: SCR_000012
Prism	GraphPad	https://www.graphpad.com/scientific-software/prism/; RRID: SCR_002798
Fiji	NIH	https://fiji.sc/; RRID: SCR_002285
Original code for analysis of sleep data	https://zenodo.org/records/12697334	https://zenodo.org/records/12697334
Other		
Free Field Speaker	Tucker- Davis Technologies, MF1	N/A
Sound-Attenuation Booth	Gretch-Ken Industries	N/A
NI board for sound generation	National Instrument	PCI-6731
Optrode	Neuronexus Technologies	A1x64-Poly2-6mm-23 s-160-OA64LP
Multi-channel silicone probe	Neuronexus Technologies	A1x64-Poly2-6mm-23 s-160-A64

EXPERIMENTAL MODEL AND SUBJECT DETAILS

All experimental procedures in this study were in accordance with the guidelines for the care and use of laboratory animals of the US National Institutes of Health (NIH) and were approved by Animal Care and Use Committee (IACUC) of the University of Southern California. The Vglut2-ires-Cre (stock # 016963), Ai14 (Cre-dependent tdTomato reporter line, stock # 007914), Fos$^{2A\text{-}iCreERT2}$ (TRAP2, stock # 030323), and C57BL/6J (stock # 000664) mice were used and obtained from the Jackson Laboratory. Mice were housed at 18−23°C with 40−60% humidity in a 12h light/dark cycle (light on at 6:00 am, light off at 18:00 pm) with ad libitum access to food and water. Experiments were performed in adult male and female mice (2−3 months old).

CellPress

METHOD DETAILS

Viral injection

AAV1-CAG-FLEX-GFP-WPRE (Addgene, 51502), AAV1-EF1a-DIO-hChR2 (H134R)-EYFP-WPRE (Addgene, 20298), AAV1-EF1a-DIO-EYFP-WPRE (Addgene, 27056), pAAV-CAG-ArchT-GFP (Addgene, 29777), pAAV-EF1a-DIO-hM4D (Gi)-mCherry (Addgene, 50461), pAAV-EF1α-DIO-mCherry (Addgene, 50462) and AAV1-Syn-FLEX-GCaMP6s-WPRE-SV4 (Addgene, 100845) were used in this study. Stereotaxic injection of viruses was conducted as we previously described.[74,75] Mice were positioned on a warming pad and anesthetized throughout the entire surgical procedure with 1.5% isoflurane (dissolved in oxygen) through inhalation. Subsequently, buprenorphine was administered subcutaneously following the induction of anesthesia. Following aseptic measures, a minor incision was made in the skin, and the muscles were gently displaced to expose the skull. For virus injection, a craniotomy window of approximately 0.2 mm in size was made over the designated target region (PCG, AP -5.5 mm, ML +0.4 mm, DV -3.2 mm), and the virus was delivered through a pulled glass micropipette with beveled tip (~20 μm diameter) by pressure injection via a micropump (World Precision Instruments). Stereotaxic coordinates of injection were based on the Allen Reference Atlas www.brain-map.org. A volume of 50 nL was administered to each injection site, and the pipette remained stationary for 5 minutes before gradual withdrawal. Following this, the scalp was sutured, and antibiotic ointment was applied to the wound. Ketoprofen was administered at a dose of 0.5 mg/kg for the three days following the surgical procedure. The viruses were expressed for a minimum of 3 weeks before behavioral or recording experiments.

Optogenetic manipulation

For optogenetic manipulations, optical fibers were implanted into the targeted region two weeks following the viral injection (PCG, bilateral implantation, AP −5.5 mm, ML +1.75 mm, DV −3.1 mm, with a 15° angle; MD, bilateral implantation, AP −1.2 mm, ML +1.5 mm, DV −3.0 mm, with a 15° angle; PVT, unilateral implantation, AP −1.2 mm, ML +0.6 mm, DV −2.7 mm; with a 10° angle; LHA, AP −1.5 mm, ML +1.2 mm, DV −4.7 mm, with a 10° angle; LPO, bilateral implantation, AP +0.2 mm, ML +1.2 mm, DV −4.5 mm, with a 10° angle; VTA, AP −3.2 mm, ML +1.5 mm, DV −4.3 mm, with a 10° angle). The animals were anesthetized with 1.5% isoflurane and underwent surgery involving the drilling of a small hole. Optic cannulas (200 μm core, NA = 0.22, RWD Inc.) were then inserted to the desired depth and secured in place using dental cement. The animals were given a one-week recovery period before the commencement of experiments. Before conducting behavioral tests, mice were acclimated to optical cables for three days without LED stimulation. To avoid any light leakage, black tape was utilized to conceal the connection point between the optical cable and the implanted ferrule. For optogenetic activation experiments, a blue LED source (470 nm, 20 Hz, 5-ms duration, Thorlabs) was used. For optogenetic silencing experiments, continuous green light (530 nm, Thorlabs) was delivered. The light intensity at the fiber tip was approximately 7-10 mW. All the control groups received the same experiment procedures and light stimulation. After each experiment, the animals were transcardially perfused and the locations of the viral expression and the track of optical fibers were examined.

Awake head-fixed animal preparation

For awake recording from head-fixed animal preparations, the procedures closely followed those described previously.[20,76,77] Mice were placed on a heating pad and anesthetized with 1.5% isoflurane. Subsequently, a screw was affixed to the surface of the skull using dental cement to facilitate head fixation. One day prior to recording, a craniotomy window was carefully crafted over the designated recording region. (MD: AP −1.2 mm, ML +0.6 mm, DV −3.1 mm; LPO: AP +0.2 mm, ML +0.5 mm, DV −4.7 mm; LHA: AP −1.5 mm, ML +1.1 mm, DV −5.1 mm; PVT: AP −1.2 mm, ML +0.6 mm, DV −2.95 mm with 10° angle; VTA: AP −3.2 mm; ML +0.3 mm; DV −4.5 mm; MRN: AP -3.0~ -4.5 mm, ML +1.3 mm, DV -3.6 mm; PCG: AP −5.5 mm, ML +0.4 mm, DV −3.1 ~ −3.4 mm). Silicone adhesive (Kwik-Cast Sealant, WPI Inc.) was applied to cover the craniotomy window until the recording sessions. Following the surgical procedures, animals were given a one-week recovery period before the recording experiments. During this time, mice were habituated to the recording setup.

Sound generation and stimuli

All experiments were conducted in a sound-attenuation booth (Acoustic Systems). The sound stimulation and data acquisition were generated by custom-written codes in LabVIEW (PCI-6731 NI board for sound generation, 16-bits output, 1MHz sampling rate, National Instruments, Austin, TX). For *in vivo* multichannel recordings, the experimental sequence remained consistent for each recorded cell: initial assessment of the response to 80 dB SPL noise (~200 trials, with a 5-s inter-stimulus interval), subsequent FRA mapping (repeated 3 times), and examination of the rate-intensity function. For FRA mapping, pure tones (2-64 kHz at 0.1-octave intervals, 50-ms duration, 3-ms ramp) at eight, 10 dB-spaced sound intensities (0-70 dB SPL) were delivered in a pseudo-random sequence. For testing the rate-intensity function, broadband white noise (2-64 kHz) at eleven intensities (0-100 dB SPL spaced at 10 dB), with the inter-stimulus interval set as 5-s. For auditory-induced awakening experiments, broadband white noise (2-64 kHz) at various intensities (30-70 dB SPL) were applied with intervals randomly chosen between 60-180 s, from an open field speaker (MF1, Tucker- Davis Technologies) placed 30 cm above the testing chamber.

EEG and EMG electrodes implantation

Two weeks following AAV viral injections, mice were implanted with EEG and EMG electrodes under isoflurane anesthesia for polysomnographic recordings. EEG and EMG signals were recorded from stainless steel screws inserted on the skull and two flexible

silver wires inserted into the neck muscle, respectively. Electrodes were connected to EEG/EMG headmounts (Omnetics, A79022-001). Optic fibers or drug cannulas were positioned bilaterally above the target region during the EEG and EMG implantation. All electrodes and optical fibers were fixed to the skull with dental cement. After surgery, mice were allowed to recover for at least one week before experiments.

EEG/EMG data acquisition, processing, and sleep-wake state classification

Following the recovery period, mice were familiarized with the recording chamber, and EEG and EMG electrodes were connected via a small connector. The Open-Ephys system was used to record and monitor the EEG and EMG signals, with a sampling rate of 1 kHz and bandpass filtered at 0.5-500 Hz. High-resolution videos were recorded, and mice underwent a 30-minute habituation period in the recording chamber with bedding materials present, before the start of data collection. Auditory-induced awakening and optogenetic experiments were conducted in a sound-attenuation room during the light cycle of animals.

For sound-induced awakening experiments, 30-70 dB SPL broadband white noise (1-s duration, with inter-stimulus intervals randomly chosen between 60-180 sec) were applied randomly at irregular intervals to prevent adaption (Figure S3A). For sound-induced awakening experiments combined with optogenetic silencing, the laser was applied for 5 s continuously. For optogenetic activation experiments, bilateral optical stimulation (20 Hz, 5-ms pulses for 20-s) was applied, repeated about every 5 minutes. Control mice underwent the same procedure. Continuous monitoring of EEG and EMG signals was performed throughout the experiments.

States were analyzed and characterized for a 5-s window, sequentially shifted by 2.5-s increments using an automated threshold algorithm. The brain states were classified into wake, NREM and REM states (wake: desynchronized EEG and high EMG activity; NREM: synchronized EEG with high-amplitude, low-frequency [0.5-4 Hz] activity and low EMG activity; REM: high power at theta frequencies [6-12 Hz] and low EMG activity).[78,79] Since EEG/EMG activity was recorded continuously for 3 hours in the chemogenetic experiments, every six consecutive 5-sec segments of categorized states was further classified into a 30-sec epoch based on the predominant states within these six 5-sec segments, thus smoothing the state fragmentation.[63,80] For sound-induced awakening, only trials conducted with the animal having been in a sleep state for at least 10-s were analyzed in this study. Successful sound-induced awakening trials were characterized by a marked desynchronization of EEG activity and increased EMG activity[73] occurring within 3.5 s after the onset of auditory stimulation and persisting for at least 3 s. If these criteria were not met, the trial was categorized as a failed awakening trial. All sleep scoring was performed by a custom MATLAB script. For EEG spectrogram, we decomposed EEG signals into time-frequency using Morlet wavelet, following a previous study.[13] Time-varying energy is then smoothed by a moving average filter with a span of 2 s for each frequency step to enhance visualization.

Anesthesia experiments

Anesthesia experiments were conducted during the dark cycle of animals. The mice were placed in a transparent and clear rectangle chamber connected to an isoflurane vaporizer. EEG and EMG electrodes were connected to flexible recording cables via a connector, and baseline EEG and EMG activities were recorded. Following 5 minutes of free exploration in the anesthesia chamber, the mice were induced with 5% isoflurane and maintained under 1.5% isoflurane anesthesia. The anesthetized state was confirmed by the loss of the righting reflex. After 20 minutes of exposure, isoflurane delivery was stopped, and optical stimulation (20 Hz, 5-ms duration) was applied until the righting reflex was regained. The control group received the same optical stimulation parameters. In experiments involving auditory-induced arousal from anesthesia, broadband white noise (70 dB SPL) was applied until the righting reflex was regained. To test the involvement of PCG glutamatergic neurons in auditory-induced arousal, continuous green LED light (530 nm) was applied alongside the sound presentation. The latency to wakefulness from anesthesia was defined as the time elapsed until EMG activity resumed. Viral expression and implantation locations were verified after the experiments.

Pharmacological silencing

For pharmacological silencing of PCG, mice underwent a drug cannula implantation surgery one week before the pharmacological manipulation. The surgery procedure was similar to optical fiber implantation as described above. Mice were anesthetized with isoflurane and a drug cannula (internal diameter: 140 μm) was implanted into the PCG (AP -5.5 mm, ML $+1.75$ mm, DV -3.1 mm, with a 15^{o} angle). A fluorescent muscimol (Bodipy Tmr-x Conjugate, 1.5 mM, Invitrogen) was infused to silence PCG. Using a thin pipette connected to a microinjector, the drug was injected into the targeted region through the implanted drug cannula. A volume of 100 nL was slowly delivered during the injection process. The evoked spiking responses were recorded and compared before and after the drug application. The mouse was perfused transcardially to examine the location of cannula and drug spread after the recording experiment.

Chemogenetic silencing

For DREADD experiments, virus encoding Cre-dependent inhibitory DREADD receptors (hM4Di) was stereotaxically injected into PCG of Vglut2-Cre mice bilaterally. To examine the role of PCG glutamatergic neuron activity in natural sleep-wake cycles, mice expressing hM4D-mCherry or mCherry alone received intraperitoneal injection of CNO (i.p., 1mg/kg) or saline (100 nL).[32] EEG and EMG recordings began 30 minutes after the drug injection and continued for 3 hours during the dark cycle (7:00 pm and 10:00 pm). Verification of viral expression was conducted post-experiment.

In vivo multichannel electrophysiological recordings

All the *in vivo* recordings were performed in a sound-attenuation room (Acoustic Systems) as previously described.[18,20] The animal was head-fixed on the recording setup and the silicon seal was removed, then a 64-channel silicon probe (A1x64-Poly2-6mm-23s-160-A64, NeuroNexus Technologies) was lowered into the target brain structure. To capture PCG glutamatergic neuron activity throughout natural sleep-wake cycles, an optrode (A1x64-Poly2-6mm-23s-160-OA64LP, the distance between the tip of the optic fiber and the probes is 200 μm, NA 0.22, Neuronexus Technologies) connected to a LED light source (480nm, Thorlabs) via an optic fiber was lowered into the target brain structure. To identify ChR2-tagged neurons, 10-Hz (5-ms pulse duration, controlled via an Arduino microcontroller) LED pulse trains were delivered intermittently. EEG and EMG signals were conducted using an Open-Ephys system simultaneously. All signals were saved for offline analysis. The silicone probe was coated with DiI (Invitrogen) to label the electrode track. Animals were transcardially perfused and the locations and tracks of the electrodes were examined.

Fiber photometry recording and data analysis

To obtain calcium signals, 480 nm LED light (Thorlabs) was bandpass filtered (ET470/24M, Chroma), focused by an objective lens (Olympus), and coupled through an optical fiber (O.D.= 400μm, NA = 0.48, 1 m long, Doric) connected to an implanted optic fiber (400μm, NA = 0.5, Thorlabs) via a ceramic sleeve. To avoid photobleaching, the LED power was set at 0.02 mW. The fluorescence calcium signal was bandpass filtered (ET525/36M, Chroma) and collected by a photomultiplier tube (H11706-40, Hamamatsu), and then passed through an amplifier (Model SR570, Stanford Research System) and low-pass filtered (30 Hz). Then the current output was converted to a voltage signal by a data acquisition card (PCI-MIO-16E-4, National Instruments). The photometry voltage signals were digitized at 250 Hz and recorded by LabView software. The EEG and EMG signals were recorded by the Open Ephys system simultaneously. Data were obtained using custom LabVIEW software and off-line analyzed using custom MATLAB scripts.

For data analysis, photometry data were exported to MATLAB for further analysis. ΔF/F was calculated as (F – F0) / F0, where F0 is the median fluorescence signal of each session. For analyzing the state transition, we determined each state transition and aligned ΔF/F in a ± 60 s window around that point was calculated.

TRAP induction

Drug preparation

4-Hydroxytamoxifen (4-OHT; Sigma, Cat# H6278) was dissolved at a concentration of 20 mg/mL in ethanol by shaking at 37°C for 15 minutes. Corn oil was then added to achieve a final concentration of 10 mg/mL 4-OHT, and the ethanol was removed by vacuum centrifugation. All injections were administered intraperitoneally (i.p.). A dosage of 50 mg/kg 4-OHT was administered in all TRAP experiments.[37,81]

Auditory stimulation

TRAP mice were housed in a sound-proof box for 12 hours. Auditory stimulation was performed in a sound-attenuation room during the light phase. The loudspeaker was placed above the animal's cage. On the TRAPing day, mice were exposed to 60 min broadband white noise (70 dB SPL, 2-64 kHz) and injected with 50 mg/kg 4-OHT (i.p.) right after auditory stimulation. Mice were returned to their homecages 12 hours after the injection 4-OHT. They were euthanized 7-9 days post-TRAPing. Control mice were treated with the same procedures but without auditory stimulation.

Histology, imaging and quantification

After completing all experiments, animals were deeply anesthetized with isoflurane and transcardially perfused with phosphate-buffered saline (PBS), followed by 4% paraformaldehyde (PFA). The brain was carefully extracted and post-fixed in 4% PFA for 24 hours at 4°C. Subsequently, the brain was coronally sectioned into 150-μm-thick slices using a vibratome (Leica Microsystems). The free-floating sections were washed three times with PBS for 10 minutes each and then stained with Nissl reagent (Neurotrace 620, ThermoFisher, N21483) and Triton-X100 (10%) (Sigma-Aldrich) for 2 hours at room temperature while being shielded from light using aluminum foil. Finally, all slices were examined using a confocal microscope (Olympus FluoView FV1000). To count the TRAPed+ cell in different brain structures, at least three 150-μm-thick sections were collected from each mouse and imaged by confocal microscope (Olympus FluoView FV1000) with a 10× objective under Z-stacks. The total number of tdTomato+ cells in each brain region were manually counted.

QUANTIFICATION AND STATISTICAL ANALYSIS

Data analysis

For multichannel recordings, spike trains were sorted offline. The signals were filtered through a bandpass filter (0.3-3 kHz). The 64-channel probes were grouped into four tetrodes and then performed semiautomatic spike sorting by using Offline Sorter (Plexon) following our previous studies.[20,25,76] To identify the units driven directly by ChR2 activation, we analyzed the onset latency of spikes relative to the onset of light stimulation. Only spikes with latency < 3-ms were considered as being directly stimulated in this study. The average waveforms were computed and compared between LED-evoked and auditory-evoked spikes. Sound responsiveness of a neuron was defined by the criterion that the evoked firing rate, measured within a 50-ms window after the stimulus onset, exceeded the average baseline firing rate (measured during the 100-ms time window before the stimulus onset) by 3 standard deviations of baseline fluctuations. The response onset latency was identified by the time point at which spiking activity first exceeded the

average baseline firing rate (measured during the 50-ms time window before the stimulus onset) by 3 standard deviations of baseline fluctuations, within 1-ms bin. FRAs were reconstructed according to the array sequence. The Z-score was calculated as the evoked firing rate (calculated within a 50-ms window after the stimulus onset) divided by the standard deviation of the baseline firing rate (calculated within a 50-ms window before the stimulus onset). To analyze the spontaneous firing rate of PCG glutamatergic neurons, the animal's brain state was first divided into wake, REM and NREM states based on the EEG and EMG signals. Then the spontaneous firing rate in PCG glutamatergic neurons was compared between different brain states.

Statistics

Shapiro–Wilk test was first used to examine whether samples had a normal distribution. In the case of a normal distribution, parametric tests were used. For two groups comparison, paired or unpaired two-tailed student's t test was used. One-way or two-way ANOVA followed by LSD or Tukey post hoc comparison was used for multiple comparisons. Significance level was marked as *: $P < 0.05$; **: $P < 0.01$; and ***: $P < 0.001$. Data are presented as mean ± SD, unless otherwise indicated. Statistical analyses were performed with GraphPad Prism version 10.